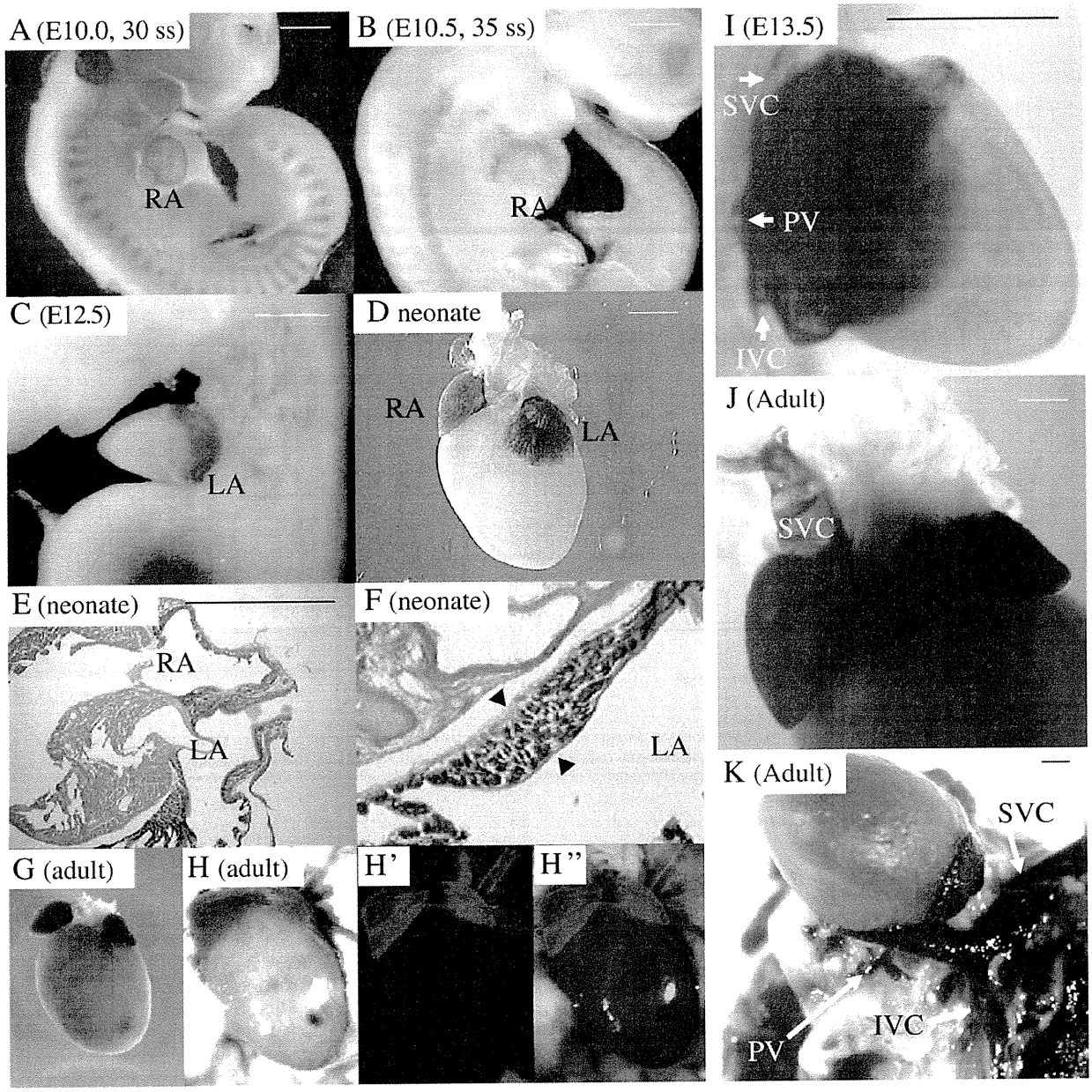

Fig. 2. *In vivo* atrial lineage tracing. (A) *In situ* hybridization for *SLN* at the 30 somite stage. *SLN* is expressed in atria and myotomes. (B–H″) Contribution of SLN^+ cells to atrial myocardium. Atrial specific labeling is shown by whole mount Xgal staining at E10.5 (B), E12.5 (C), neonatal (D) and adult (G) stages, and section Xgal staining of neonatal hearts (E, F) of *SLN-cre; R26R* mice. Note that the vast majority of the atrial myocytes are labeled. As indicated by black arrowheads, there were no Xgal-positive cells in endocardium or epicardium. H, H′ and H″ show the hearts from adult *SLN-cre; CAG-DsRed reporter* mice. The expression of βgal and DsRed reporters is restricted to atrial myocytes throughout cardiogenesis and in the adult heart. Scale bar = 1 mm. (I–K) Contribution of SLN^+ cells to the cardiac inflow tract. Whole mount Xgal staining of the inflow tract of $SLN^{cre/+}$; *R26R* embryo at E13.5 (I) and adult heart (J, K) shows that the proximal part of the SVC, IVC and PV are derived from SLN-positive cells (white arrows in I and K). Scale bar = 1 mm. IVC, inferior vena cava; LA, left atrium; PV, pulmonary vein; RA, right atrium; SVC, superior vena cava.

cardiac cells in the atrial chamber and sinus venosus have already started to express SLN, and some are positive for both Isl1 and SLN (Fig. 4A, black arrows). At E13.5, $Isl1^+$ cells in the splanchnic mesoderm are still negative for SLN (Fig. 4B, black arrowheads), although most of the atrial myocytes were already positive for βgal activity. $Isl1^+/SLN^+$ cells were still found in dorsal mesenchymal protrusion (Fig. 4B, black arrows) [15,23–28]. These cells gradually lose Isl1 expression and progressively acquire SLN as they migrate towards the cushion (Fig. 4B, black arrows). These data suggest that a subset of $Isl1^+$ cells give rise to SLN^+ atrial myocytes, and that $Isl1^+/SLN^+$ cells represent a transient cell population that are committed to the mature atrial myocyte fate.

3.4. Single $Isl1^+/SLN^+$ cells give rise to both cardiac and smooth muscle cells

To examine whether cardiac and smooth muscle lineages can originate from a single common $Isl1^+/SLN^+$ cell, we dissected forming atrial tissue from E9.5 $SLN^{cre/+}$; *R26R* embryos, dissociated them into single cells and cultured them at clonal density on cardiac mesenchymal feeder layers as previously described (Fig. 5A) [2,29,30]. βGal-labeled atrial cells grew to form colonies, and more than 90% of them were positive for Isl1 (Figs. 5B, D and Supplementary Table 2). Using a *CAG-DsRed reporter* line [22], the atrial progenitor colonies were

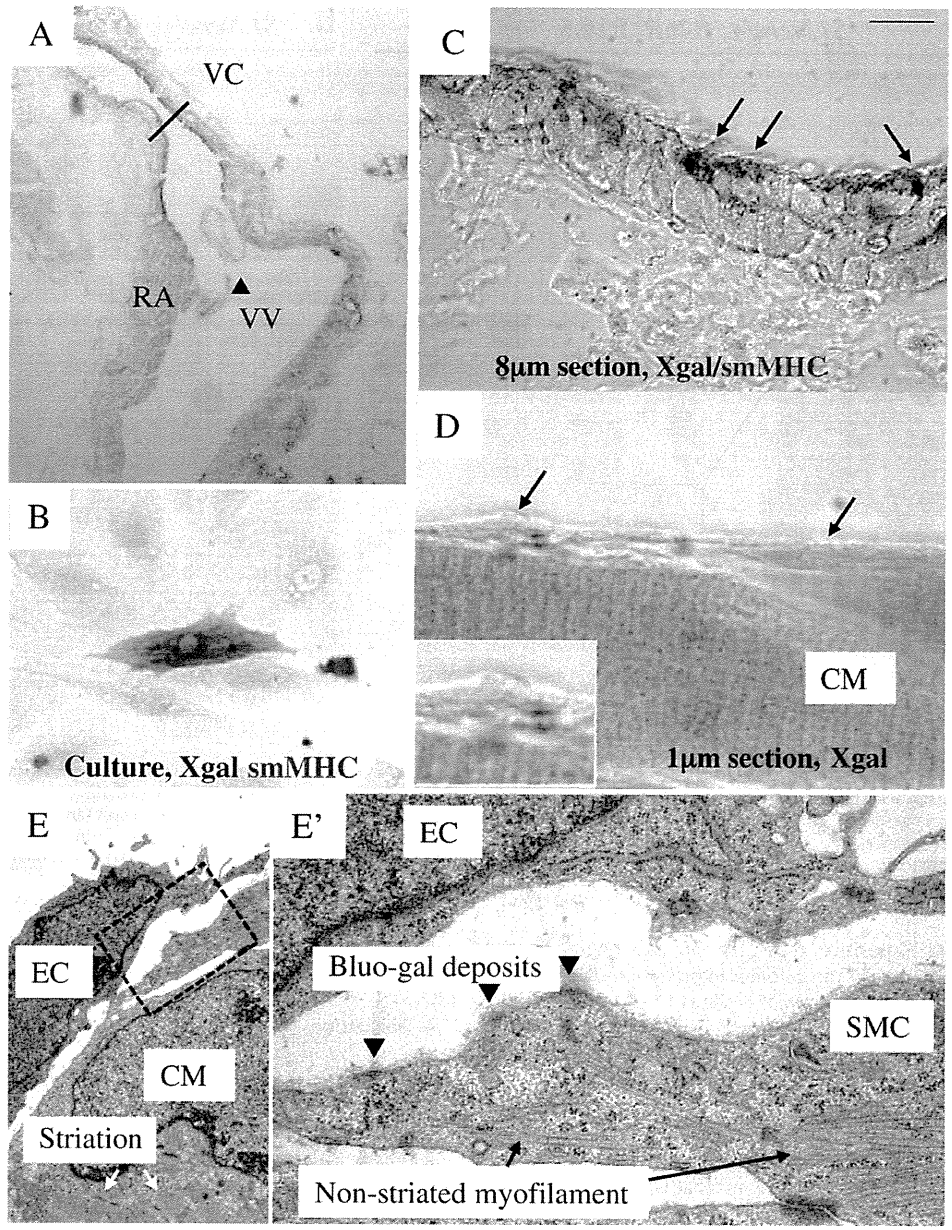

Fig. 3. SLN-positive cells give rise to smooth muscle cells in the cardiac inflow tract. (A) Low magnification view of the junction between right atrium and vena cava of adult *SLN*$^{cre/+}$; *R26R* mouse co-stained with Xgal and smMHC. The proximal region of the vena cava (VC) consists of two muscular layers; Xgal-positive outer myocardial layer (blue) and smMHC-positive inner smooth muscle layer (brown), and demarcated from the right atrium (RA) by venous valves (VV, arrowhead) which are also derived from SLN-positive cells. (B) Expression of a smooth muscle marker in βgal-labeled cells isolated from the cardiac inflow region of adult *SLN*$^{cre/+}$; *R26R* mice. Tissues from the vena cava of adult *SLN*$^{cre/+}$; *R26R* mouse were dissociated and plated onto a culture dish. Some cells express both βgal (blue) and smMHC (brown), suggesting that a fraction of SLN-positive cells gave rise to smooth muscle cells in the inflow tract. (C) Smooth muscle cells derived from SLN-expressing cells. Light microscopic analysis of 8 μm sections shows the smMHC-positive cells in the inner layer co-stained with Xgal (scale bar = 50 μm). Sections were cut along the line indicated in A. (D) 1 μm sections show clear Xgal staining on smooth muscle cells (arrows) between a thin endothelial layer and a thick myocardial layer (CM) (scale bar = 20 μm). Sections were cut along the line indicated in A. (E, E′) Electron microscopic analysis (×49,500) of the vena cava of adult *SLN*$^{cre/+}$; *R26R* mouse stained with Bluo-gal. Bluo-gal deposits (arrowheads) are found in smooth muscle cells (SMC) with non-striated myofilaments (black arrows). Note that the cardiomyocytes have striated myofilaments (white arrow). CM, cardiomyocyte; col, collagen fiber; EC, endothelial cell; SMC, smooth muscle cell; MF, myofilament; RA, right atrium; VC, vena cava; VV, venous valve.

visualized alive (Fig. 5C), picked up under the fluorescent microscope, and examined for their mRNA expression signature. After 3–4 days on feeders, the majority of the clones (early-stage colonies) were positive for early cardiac markers (Isl1, Nkx2.5, and GATA4) and atrial markers (SLN and MLC2a) (Fig. 5D). However, the expression of ANF and smMHC were only occasionally found at this stage. Therefore, the feeder system is useful for propagating immature atrial cells *in vitro*.

After differentiation for 7–12 days in culture, most of the βgal-labeled cells express cTnT. However, cTnT-negative cells were also found in the periphery of the βgal-labeled colonies (Fig. 5E, black arrow). These peripheral cells were co-stained with Xgal/smMHC (Fig. 5E, white arrows). RT-PCR revealed that no colony was positive for Isl1 at this stage (Fig. 5G). Whereas all the clones examined gave rise to cTnT-positive cardiomyocytes, 51.3% of them were capable of

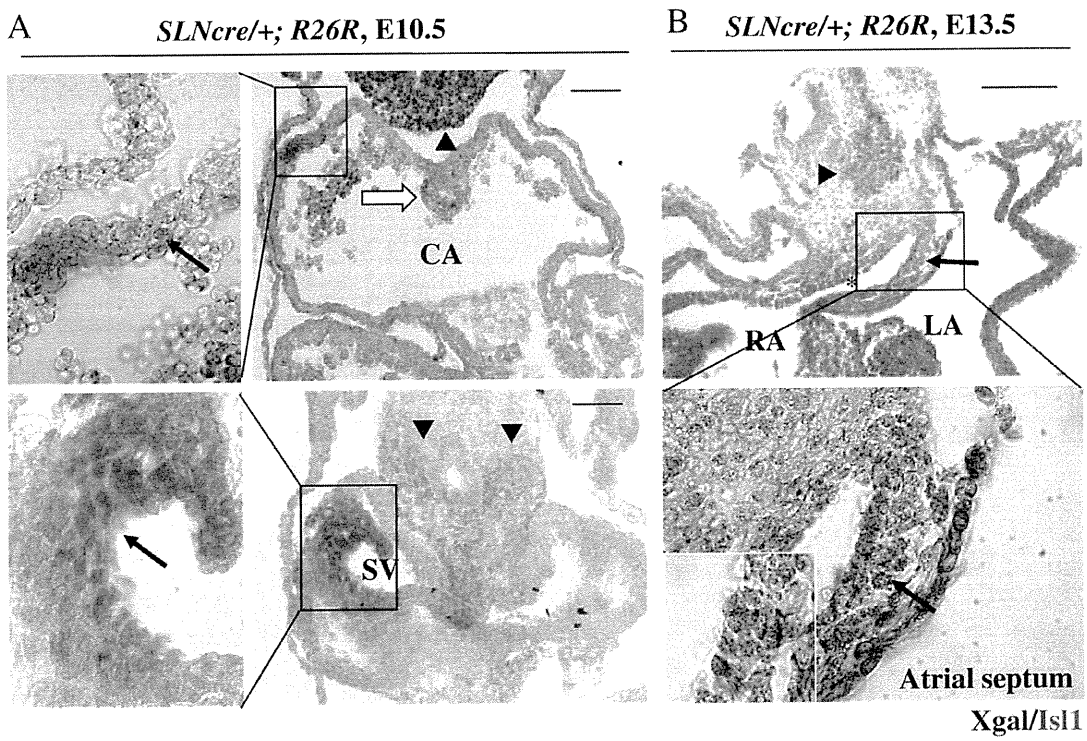

Fig. 4. Identification of Isl1^{+}/SLN^{+} cells during cardiogenesis. Heart sections from *SLN$^{cre/+}$; R26R* embryo at E10.5 (A) and E13.5 (B) were double-stained for Xgal and Isl1. Scale bar = 100 μm. (A) At E10.5, most of the Isl1-positive cells in forming atria are negative for Xgal. Whereas cells in the splanchnic mesoderm (black arrowheads) and primary atrial septum (white arrow) strongly express Isl1, Xgal-positive cells with a weaker level of Isl1 are also seen in atrial free wall and sinus venosus (arrows). (B) At E13.5, most of the atrial myocytes have already started to express SLN. Isl1-positive immature cardiac progenitors in the splanchnic mesoderm (arrowhead) migrate into the septum and start to express SLN while maintaining Isl1 expression (black arrow). During the migration, atrial cells gradually lose Isl1 expression and gradually express SLN. CA, common atrium; LA, left atrium; RA, right atrium; SV, sinus venosus.

giving rise to smMHC-positive cells (Fig. 5G and Supplementary Table 2). Given that 90.3% of the colonies express both Isl1 and SLN, these data suggest that more than half of the Isl1^{+}/SLN^{+} cells at E9.5 are capable of giving rise to both cardiac and smooth muscle cells. To examine the destination of Isl1^{+}/SLN^{+} cells, DsRed-labeled cells were propagated for 7–12 days on feeders, and FACS-sorted onto glass slides by cytospin for smooth muscle staining. As shown in Fig. 5H, 3.1% of the progeny of atrial cells gave rise to smMHC-positive smooth muscle cells *ex vivo* consistent with *in vivo* lineage tracing data (Supplemental Table 1). These data suggest that while more than half of Isl1^{+}/SLN^{+} cells are smooth muscle competent, not all of them actually give rise to smooth muscle cells.

Interestingly, atrial colonies derived from a later stage (E12.5 and 15.5) showed a decrease in smooth muscle differentiation capability (Supplementary Table 2), suggesting that smooth muscle competency is gradually restricted as the atrial myocytes mature.

Taken together, these data suggest that Isl1-positive cells in the atrial lineage contribute to cardiac as well as smooth muscle cells in the cardiac inflow tract during migration from splanchnic mesoderm.

In conclusion, we reported (1) a novel Cre mouse line which specifically and sensitively labels the atrial cardiac lineage, (2) the developmental contribution of the atrial cells into the smooth muscle cells in cardiac inflow tract, (3) the smooth muscle competency of immature atrial cells, and (4) the gradual loss of smooth muscle competency during cardiogenesis. Together, these findings provide an insight into the mechanism underlying the formation of the boundary between atrial myocardium and vascular smooth muscle layer. The myocardial–smooth muscle junction in the vena cava is often affected in some types of congenital heart disease. Moreover, the myocardial sleeve in pulmonary vein is highly arrhythmogenic in diseased and/or aged hearts. Elucidating how the plasticity of heart progenitors serves the cardiovascular morphogenesis will provide a better understanding of the pathogenesis of these diseases.

4. Discussion

The heart is the first functional organ that develops during embryogenesis, and it is unique in that it has to be operational while it is still forming. Therefore, the embryonic heart needs to strike a delicate balance between its formation and its functionality, which accounts for the fact that 1% of human live births are complicated by congenital heart diseases. A major question in cardiogenesis research is how this balance is regulated at the cellular level.

Using a newly generated atrial specific SLN-Cre knockin mouse line, we have demonstrated that the atrial subset of Isl1-positive SHF progenitors are capable of giving rise to both cardiac and smooth muscle cells until unexpectedly later stages. During the migration from splanchnic mesoderm, a majority of Isl1^{+}/SLN^{+} cells contribute to the atrial myocardium, while a subset of them are incorporated into the inner layer of the inflow tract and give rise to smooth muscle cells (Fig. 6). Instead of making binary cell fate decision at certain developmental stages, our data suggest that the atrial cells gradually lose their plasticity during cardiogenesis.

4.1. Diversification of atrial cell populations

The SHF has been characterized by several different techniques; dye injection, detection of specific markers and retrospective single cell fate tracing experiments. Different methods and different markers have determined slightly different populations of the cardiac lineages [8,10–12,31]. Atrial cells arise from the posterior part of Isl1-positive heart field [16,27,28]. The Isl1^{+}/SLN^{+} progenitors represent

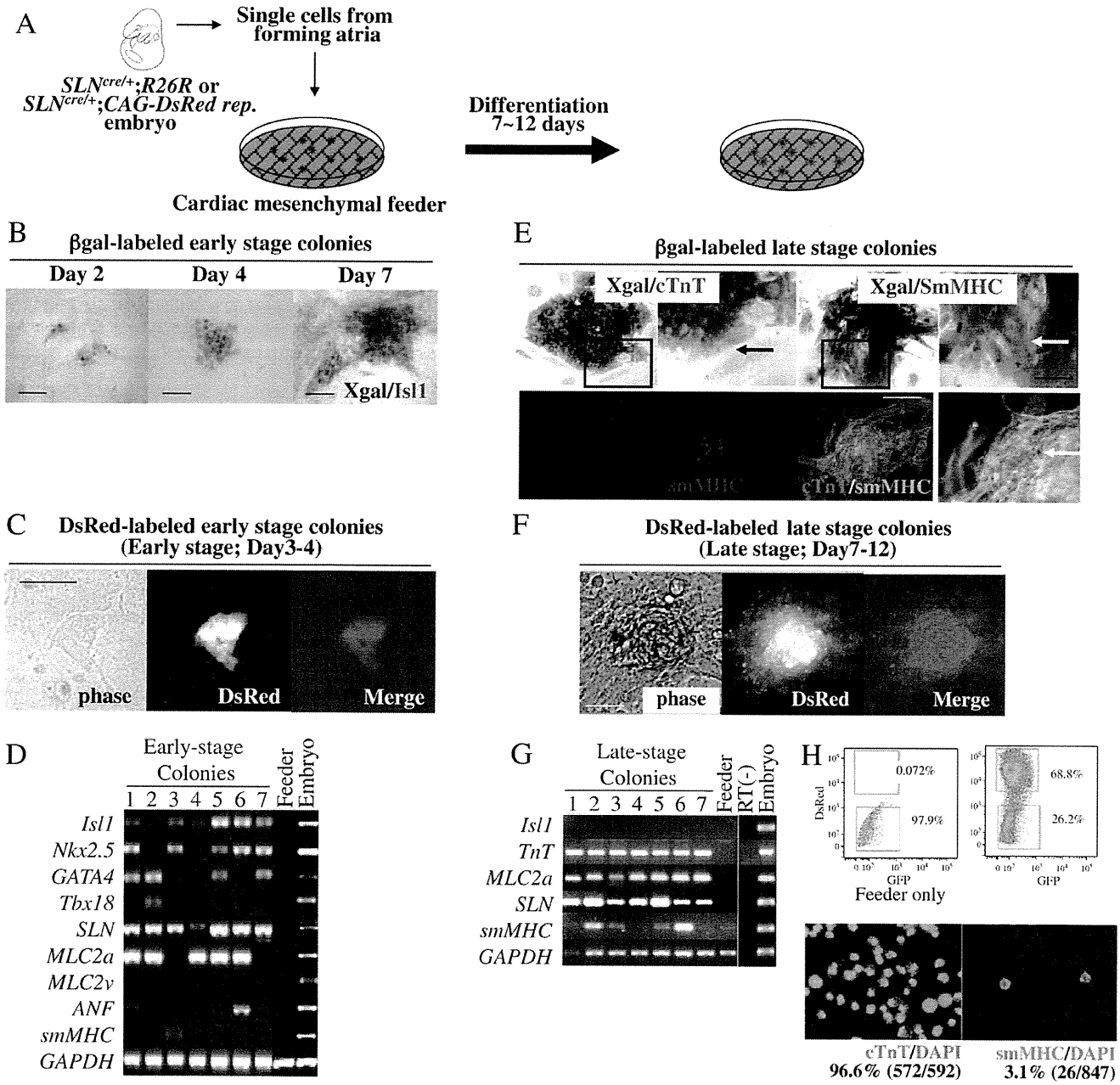

Fig. 5. Isl1^{+}/SLN^{+} cells clonally give rise to cardiac and smooth muscle cells. (A) The forming atria of E9.5 *SLN$^{cre/+}$ × R26R* or *SLN$^{cre/+}$ × CAG-DsRed reporter* embryos are dissected and dissociated with collagenase. βGal- or DsRed-labeled atrial progenitors are cultured on cardiac mesenchymal feeders at clonal density. The dissociated atrial tissues are grown for 7–12 days and then examined for cardiac and smooth muscle marker expression. (B) Colonies are stained for Isl1 at early stages (2, 4 and 7 days after isolation). βGal-labeled atrial cells maintain Isl1 expression up to 7 days on a cardiac mesenchymal feeder layer. Scale bar = 50 μm. (C) DsRed-labeled atrial progenitor colonies grown for 4 days on feeders. (D) DsRed-labeled atrial progenitors are manually picked up 4 days after isolation, and examined for marker expression by RT-PCR. Shown are 7 representative colonies. Most of the colonies expressed early cardiac markers (Isl1, Nkx2.5 and GATA4) and atrial markers (SLN and MLC2a). None of them are positive for MLC2v. At this stage, only few colonies expressed smMHC. (E) βGal-labeled atrial progenitors are differentiated for 7–12 days and stained for Xgal, cTnT and/or smMHC. Whereas most of the cells in Xgal-positive colonies were positive for cTnT, some in the periphery were negative (black arrow). These peripheral cells are co-stained with smMHC (white arrows). Lower panels show cTnT/smMHC immunofluorescent staining of a representative colony, indicating that these two cell types differentiate from a single cell (white arrow). (F) DsRed-labeled atrial colonies grown for 12 days on feeders. (G) Expression profile of atrial colonies. After 7–12 days (late stage) on feeders, colonies were picked up and examined for marker expression. RT-PCR revealed that Isl1 is already downregulated at this stage but SLN and MLC2a are still positive. Importantly, smMHC becomes positive in more than half of the colonies. (H) *Ex vivo* quantification of the percentage of smooth muscle cells derived from atrial lineage. After 7–12 days (late stage) on feeders, DsRed-labeled atrial colonies were FACS-sorted, attached on glass slides by cytospin, and stained for cTnT (left bottom panel) or smMHC (right bottom panel). Note that 3.1% of the progeny of atrial colonies were smooth muscle cells, while 96.6% were cardiomyocytes.

components of the posterior region of the secondary heart field [32], and retain proliferative activity [33] and bipotency until later stages of cardiogenesis, which apparently relates to their generation of the myocardial/smooth muscle sleeves that serve as the junctional boundary to connect the great vessels and the cardiac chambers into a functional syncytium. Interestingly, there are several diseases of the atrium and inflow tract, including a common form of congenital heart disease where the pulmonary venous inflow tract is ectopic or absent, and atrial fibrillation that relates to a reemergence of ectopic electrical activity in the pulmonary veins. The finding of bipotent

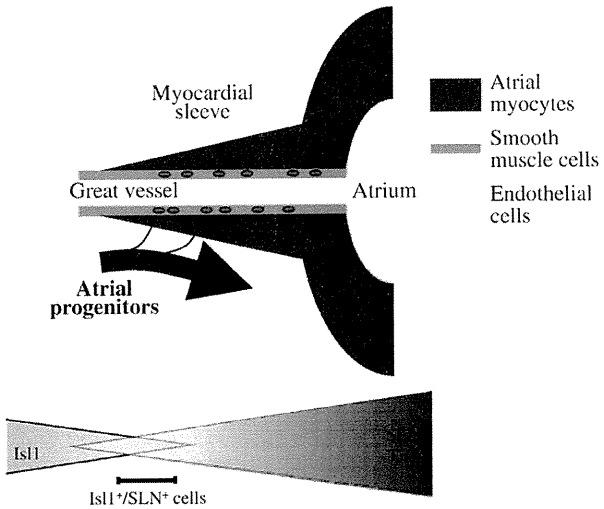

Fig. 6. A model for the migration of atrial progenitors. During the migration from the splanchnic mesoderm, Isl1-progentiors in the pSHF gradually lose Isl1 expression and start to express atrial specific markers including SLN. The Isl1$^+$/SLN$^+$ cells represent a transient cell population that is already committed to the atrial lineage, but still maintain proliferative and migratory activities. Isl1$^+$/SLN$^+$ cells mainly contribute to atrial myocardium, but some contribute to smooth muscle cells in the cardiac inflow tract. This smooth muscle competency is gradually lost during the migration and maturation.

Isl1$^+$/SLN$^+$ cells suggests the possibility that some of atrial diseases might arise from dys-regulation of the bipotency in atrial lineages.

The Isl1$^+$/SLN$^+$ atrial progenitor population includes at least three populations; working atrial myocytes, Nkx2.5$^-$/Tbx18$^+$ cardiac progenitors in the sinus venosus and mediastinal myocardium in the dorsal mesocardium [16,23,24,33–35]. These three populations derive from Isl1$^+$ posterior SHF progenitors and eventually acquire SLN expression, although our experiments cannot tell which population display smooth muscle competency. Discovery of earlier and later markers will help establish the lineage tree of the posterior SHF/venous pole population.

4.2. Lineage proximity of cardiac and smooth muscle cells

Smooth muscle cells appear to be recruited locally from a wide range of mesodermal tissues and differentiate in response to specific local signals. Our data suggest that during the migration from the posterior part of the SHF, Isl1$^+$/SLN$^+$ cells mainly contribute to mature atrial myocytes, but some cells escape from the cardiac lineage and give rise to the smooth muscle cells in the inflow tract (Fig. 6). Given that SLN is a relatively late marker of the atrial lineage, it is not unexpected that SLN$^+$ cells contribute only to 5–10% of the inflow smooth muscle cells. It is rather significant in that atrial cells give rise to smooth muscle cells *in vivo* even after the expression of SLN gene, which is involved in atrial specific contractile function [17,18].

It has been known that cardiac cells can transdifferentiate into smooth muscle cells even at the postnatal stage at low frequency upon certain culture conditions. However, little is known as to whether it is a dedifferentiation–redifferentiation process or a direct transition from differentiated cardiomyocyte to differentiated smooth muscle cell. Wu et al. reported that Nkx2.5-positive cardiac progenitors downregulate Nkx2.5 before committing to smooth muscle lineage [3]. Since Nkx2.5 is also expressed in atrial lineage, it is likely that atrial cells shut of cardiac transcriptional program in order to give rise to smooth muscle cells. Although our study cannot give a clear answer to this question, it raises the possibility that the smooth muscle competency of the postnatal myocytes may be a trace of the developmental potential of the embryonic cardiac progenitors and myocytes.

A fundamental question relates to how the smooth muscle differentiation of cardiac progenitors serves to coordinate the morphogenesis of the atrial chamber and great vessels. An interesting speculation is that the smooth muscle competency of the atrial cells is required to anchor the great veins to the atrial chambers. Malconnection of myocardium and vascular walls causes various types of congenital and adult heart diseases including anomalous pulmonary venous return and cor triatriatum [36]. In the aging and/or diseased hearts, the junctions between pulmonary veins and left atrium are highly arrhythmogenic and can be the foci of atrial fibrillation, one of the major causes of thromboembolic stroke [37–41]. Likewise, the heart-vessel junction at the arterial pole of the heart is often affected by various congenital malformations and acquired diseases including DeBakey Type I and II aortic dissection. It would be of great interest to analyze the pathogenesis of these congenital and acquired heart diseases from the viewpoint of progenitor cell plasticity.

Disclosures

None declared.

Acknowledgments

This work is supported by NIH, Jean Le Ducq foundation, Harvard Stem Cell Institute, Massachusetts General Hospital, UCLA, and Eli and Edythe Broad Center of Regenerative Medicine and Stem Cell Research. We thank Marianne Cilluffo at the Electron Microscopic Lab in Brain Research Institute, UCLA.

Appendix A. Supplementary data

Supplementary data to this article can be found online at doi:10.1016/j.yjmcc.2010.10.009.

References

[1] Kattman SJ, Huber TL, Keller GM. Multipotent flk-1$^+$ cardiovascular progenitor cells give rise to the cardiomyocyte, endothelial, and vascular smooth muscle lineages. Dev Cell 2006;11:723–32.
[2] Moretti A, Caron L, Nakano A, Lam JT, Bernshausen A, Chen Y, et al. Multipotent embryonic isl1$^+$ progenitor cells lead to cardiac, smooth muscle, and endothelial cell diversification. Cell 2006;127:1151–65.
[3] Wu SM, Fujiwara Y, Cibulsky SM, Clapham DE, Lien CL, Schultheiss TM, et al. Developmental origin of a bipotential myocardial and smooth muscle cell precursor in the mammalian heart. Cell 2006;127:1137–50.
[4] Yang L, Soonpaa MH, Adler ED, Roepke TK, Kattman SJ, Kennedy M, et al. Human cardiovascular progenitor cells develop from a KDR$^+$ embryonic-stem-cell-derived population. Nature 2008;453:524–8.
[5] Garry DJ, Olson EN. A common progenitor at the heart of development. Cell 2006;127:1101–4.
[6] Kattman SJ, Adler ED, Keller GM. Specification of multipotential cardiovascular progenitor cells during embryonic stem cell differentiation and embryonic development. Trends Cardiovasc Med 2007;17:240–6.
[7] Martin-Puig S, Wang Z, Chien KR. Lives of a heart cell: tracing the origins of cardiac progenitors. Cell Stem Cell 2008;2:320–31.
[8] Cai CL, Liang X, Shi Y, Chu PH, Pfaff SL, Chen J, et al. Isl1 identifies a cardiac progenitor population that proliferates prior to differentiation and contributes a majority of cells to the heart. Dev Cell 2003;5:877–89.
[9] Laugwitz KL, Moretti A, Caron L, Nakano A, Chien KR. Islet1 cardiovascular progenitors: a single source for heart lineages? Development 2008;135:193–205.
[10] Kelly RG, Brown NA, Buckingham ME. The arterial pole of the mouse heart forms from Fgf10-expressing cells in pharyngeal mesoderm. Dev Cell 2001;1:435–40.
[11] Mjaatvedt CH, Nakaoka T, Moreno-Rodriguez R, Norris RA, Kern MJ, Eisenberg CA, et al. The outflow tract of the heart is recruited from a novel heart-forming field. Dev Biol 2001;238:97–109.
[12] Waldo KL, Kumiski DH, Wallis KT, Stadt HA, Hutson MR, Platt DH, et al. Conotruncal myocardium arises from a secondary heart field. Development 2001;128:3179–88.
[13] Dodou E, Verzi MP, Anderson JP, Xu SM, Black BL. Mef2c is a direct transcriptional target of ISL1 and GATA factors in the anterior heart field during mouse embryonic development. Development 2004;131:3931–42.
[14] Waldo KL, Hutson MR, Ward CC, Zdanowicz M, Stadt HA, Kumiski D, et al. Secondary heart field contributes myocardium and smooth muscle to the arterial pole of the developing heart. Dev Biol 2005;281:78–90.

[15] Sun Y, Liang X, Najafi N, Cass M, Lin L, Cai CL, et al. Islet 1 is expressed in distinct cardiovascular lineages, including pacemaker and coronary vascular cells. Dev Biol 2007;304:286–96.
[16] Galli D, Dominguez JN, Zaffran S, Munk A, Brown NA, Buckingham ME. Atrial myocardium derives from the posterior region of the second heart field, which acquires left–right identity as Pitx2c is expressed. Development 2008;135:1157–67.
[17] Odermatt A, Taschner PE, Scherer SW, Beatty B, Khanna VK, Cornblath DR, et al. Characterization of the gene encoding human sarcolipin (SLN), a proteolipid associated with SERCA1: absence of structural mutations in five patients with Brody disease. Genomics 1997;45:541–53.
[18] Minamisawa S, Wang Y, Chen J, Ishikawa Y, Chien KR, Matsuoka R. Atrial chamber-specific expression of sarcolipin is regulated during development and hypertrophic remodeling. J Biol Chem 2003;278:9570–5.
[19] Babu GJ, Bhupathy P, Carnes CA, Billman GE, Periasamy M. Differential expression of sarcolipin protein during muscle development and cardiac pathophysiology. J Mol Cell Cardiol 2007;43:215–22.
[20] Xu H, Chen L, Baldini A. *In vivo* genetic ablation of the periotic mesoderm affects cell proliferation survival and differentiation in the cochlea. Dev Biol 2007;310:329–40.
[21] Soriano P. Generalized lacZ expression with the ROSA26 Cre reporter strain. Nat Genet 1999;21:70–1.
[22] Vintersten K, Monetti C, Gertsenstein M, Zhang P, Laszlo L, Biechele S, et al. Mouse in red: red fluorescent protein expression in mouse ES cells, embryos, and adult animals. Genesis 2004;40:241–6.
[23] Soufan AT, van den Hoff MJ, Ruijter JM, de Boer PA, Hagoort J, Webb S, et al. Reconstruction of the patterns of gene expression in the developing mouse heart reveals an architectural arrangement that facilitates the understanding of atrial malformations and arrhythmias. Circ Res 2004;95:1207–15.
[24] Anderson RH, Brown NA, Moorman AF. Development and structures of the venous pole of the heart. Dev Dyn 2006;235:2–9.
[25] Mommersteeg MT, Soufan AT, de Lange FJ, van den Hoff MJ, Anderson RH, Christoffels VM, et al. Two distinct pools of mesenchyme contribute to the development of the atrial septum. Circ Res 2006;99:351–3.
[26] Moorman AF, Christoffels VM, Anderson RH, van den Hoff MJ. The heart-forming fields: one or multiple? Philos Trans R Soc Lond B Biol Sci 2007;362:1257–65.
[27] Snarr BS, O'Neal JL, Chintalapudi MR, Wirrig EE, Phelps AL, Kubalak SW, et al. Isl1 expression at the venous pole identifies a novel role for the second heart field in cardiac development. Circ Res 2007;101:971–4.
[28] Snarr BS, Wirrig EE, Phelps AL, Trusk TC, Wessels A. A spatiotemporal evaluation of the contribution of the dorsal mesenchymal protrusion to cardiac development. Dev Dyn 2007;236:1287–94.
[29] Kruithof BP, van den Hoff MJ, Wessels A, Moorman AF. Cardiac muscle cell formation after development of the linear heart tube. Dev Dyn 2003;227:1–13.
[30] Bu L, Jiang X, Martin-Puig S, Caron L, Zhu S, Shao Y, et al. Human ISL1 heart progenitors generate diverse multipotent cardiovascular cell lineages. Nature 2009;460:113–7.
[31] Dyer LA, Kirby ML. The role of secondary heart field in cardiac development. Dev Biol 2009;336:137–44.
[32] Buckingham M, Meilhac S, Zaffran S. Building the mammalian heart from two sources of myocardial cells. Nat Rev Genet 2005;6:826–35.
[33] Soufan AT, van den Berg G, Ruijter JM, de Boer PA, van den Hoff MJ, Moorman AF. Regionalized sequence of myocardial cell growth and proliferation characterizes early chamber formation. Circ Res 2006;99:545–52.
[34] Christoffels VM, Mommersteeg MT, Trowe MO, Prall OW, de Gier-de Vries C, Soufan AT, et al. Formation of the venous pole of the heart from an Nkx2-5-negative precursor population requires Tbx18. Circ Res 2006;98:1555–63.
[35] Mommersteeg MT, Brown NA, Prall OW, de Gier-de Vries C, Harvey RP, Moorman AF, et al. Pitx2c and Nkx2-5 are required for the formation and identity of the pulmonary myocardium. Circ Res 2007;101:902–9.
[36] Nakano A, Nakano H, Chien KR. Multipotent islet-1 cardiovascular progenitors in development and disease. Cold Spring Harb Symp Quant Biol 2008;73:297–306.
[37] Jais P, Haissaguerre M, Shah DC, Chouairi S, Gencel L, Hocini M, et al. A focal source of atrial fibrillation treated by discrete radiofrequency ablation. Circulation 1997;95:572–6.
[38] Haissaguerre M, Jais P, Shah DC, Takahashi A, Hocini M, Quiniou G, et al. Spontaneous initiation of atrial fibrillation by ectopic beats originating in the pulmonary veins. N Engl J Med 1998;339:659–66.
[39] Haissaguerre M, Shah DC, Jais P, Hocini M, Yamane T, Deisenhofer I, et al. Electrophysiological breakthroughs from the left atrium to the pulmonary veins. Circulation 2000;102:2463–5.
[40] Chen PS, Chou CC, Tan AY, Zhou S, Fishbein MC, Hwang C, et al. The mechanisms of atrial fibrillation. J Cardiovasc Electrophysiol 2006;17(Suppl 3):S2–7.
[41] Ocorr K, Reeves NL, Wessells RJ, Fink M, Chen HS, Akasaka T, et al. KCNQ potassium channel mutations cause cardiac arrhythmias in Drosophila that mimic the effects of aging. Proc Natl Acad Sci U S A 2007;104:3943–8.

European Journal of Pharmacology 649 (2010) 263–267

Contents lists available at ScienceDirect

European Journal of Pharmacology

journal homepage: www.elsevier.com/locate/ejphar

Cardiovascular Pharmacology

Effects of *S*(+)-efonidipine on the rabbit sinus node action potential and calcium channel subunits $Ca_V1.2$, $Ca_V1.3$ and $Ca_V3.1$

Hikaru Tanaka [a,*], Iyuki Namekata [a], Toru Ogawa [a], Yayoi Tsuneoka [a], Chisa Komikado [a], Akira Takahara [a], Naoko Iida-Tanaka [a,b], Hiroko Izumi-Nakaseko [c], Hiromichi Tsuru [c], Satomi Adachi-Akahane [c]

[a] Department of Pharmacology, Toho University Faculty of Pharmaceutical Sciences, Funabashi, Chiba 274-8510, Japan
[b] Department of Food Science, Faculty of Home Economics, Otsuma Woman's University, Chiyoda-ku, Tokyo 102-8357, Japan
[c] Department of Pharmacology, Toho University Faculty of Medicine, Ohta-ku, Tokyo 143-8540, Japan

ARTICLE INFO

Article history:
Received 25 December 2009
Received in revised form 10 August 2010
Accepted 7 September 2010
Available online 19 September 2010

Keywords:
S(+)-efonidipine
Sinus node
Calcium channel
$Ca_V1.3$

ABSTRACT

The effect of *S*(+)-efonidipine on sinus node action potential and calcium channel α-subunits was examined. The slope of the phase 4 depolarization of isolated rabbit sinus node tissue was significantly reduced by *S*(+)-efonidipine (1 μM), slightly reduced by nifedipine (1 μM), but was not affected by *R*(−)-efonidipine. *S*(+)-efonidipine (1 μM), inhibited the expressed $Ca_V1.2$, $Ca_V1.3$ and $Ca_V3.1$ channel currents by 75.7%, 75.3% and 94.0%, nifedipine 84.0%, 43.2% and 14.9%, and *R*(−)-efonidipine 30.0%, 19.6% and 92.8%, respectively. Thus, the prolongation of the phase 4 depolarization of the rabbit sinus node by *S*(+)-efonidipine may be explained by blockade of the $Ca_V1.3$ channel current.

1. Introduction

Efonidipine is an antihypertensive and antianginal drug with dihydropyridine structure, which was developed as an antihypertensive agent with slow onset and long duration of action. It has excellent clinical profiles such as moderate reduction of heart rate (Masuda and Tanaka, 1994; Shimizu et al, 2001; Tanaka and Shigenobu, 2002; Tanaka et al., 2007; Morimoto et al., 2009; Ohashi et al., 2009). Studies with rabbit isolated sinus node preparations revealed that efonidipine prolongs the phase 4 (diastolic) depolarization leading to reduction of heart rate, which could be explained through its dual blocking effect on L-type and T-type Ca^{2+} channels (Masumiya et al., 1997, 1998; Tanaka and Shigenobu, 2005). Recently, however, the *R*(−)-enantiomer of efonidipine, which selectively blocks the T-type Ca^{2+} channel (Furukawa et al., 2004; Tanaka et al., 2004), was shown to have no prolonging effect on the phase 4 depolarization of the rabbit isolated sinus node (Tanaka et al., 2008). This observation raised the possibility that the prolonging effect of efonidipine on the phase 4 depolarization of this preparation originates in the *S*(+)-enantiomer, and that mechanisms other than T-type Ca^{2+} channel inhibition might be involved. Concerning L-type Ca^{2+} channels, an α-subunit encoded by $Ca_V1.3$, which activates at more negative voltage than that encoded by $Ca_V1.2$, has been postulated to contribute to the phase 4 depolarization of the sinus node based on experiments with $Ca_V1.3$ deficient mice (Platzer et al., 2000; Koschak et al., 2001; Zhang et al., 2002; Mangoni et al., 2003; Ono and Iijima, 2005).

In the present study, we examined the effects of *S*(+)-efonidipine on the rabbit sinus node action potential to clarify whether the prolongation of phase 4 depolarization by racemic efonidipine can be ascribed to the *S*(+)-enantiomer. Further, to obtain information on its mechanism of action, we examined the effects of *S*(+)-efonidipine on Ca^{2+} channel α-subunits $Ca_V1.2$, $Ca_V1.3$ and $Ca_V3.1$, and compared them with the effects of nifedipine and *R*(−)-efonidipine.

2. Materials and methods

2.1. Action potential measurements

The present study was approved by the Ethics Committee of Toho University, and was conducted in accordance with the Guiding "Principles for the Care and Use of Laboratory Animals Approved by The Japanese Pharmacological Society". Standard glass microelectrode experiments were performed with isolated rabbit sinus node tissue as in our previous study (Masumiya et al., 1997; Tanaka et al., 2008). Male rabbits weighing 2 to 3 kg were anesthetized with sodium pentobarbital (30 mg/kg) and the hearts were quickly isolated. Tissue including the sinus node were cut perpendicularly to the crista terminalis into strips

* Corresponding author. Department of Pharmacology, Toho University Faculty of Pharmaceutical Sciences, Miyama 2-2-1, Funabashi, Chiba 274-8510, Japan. Tel.: +81 474722092; fax: +81 474722113.
E-mail address: htanaka@phar.toho-u.ac.jp (H. Tanaka).

0014-2999/$ – see front matter © 2010 Elsevier B.V. All rights reserved.
doi:10.1016/j.ejphar.2010.09.014

of about 1×3 mm. Preparations were pinned down horizontally on a silicon block in a 20 ml organ bath containing physiological salt solution of the following composition (mM concentration): NaCl, 118.4; KCl, 4.7; $CaCl_2$, 2.5; $MgSO_4$, 1.2; KH_2PO_4, 1.2; $NaHCO_3$, 24.9; and glucose, 11.1 (gassed with 95% O_2–5% CO_2, pH 7.4). The temperature of the organ bath was maintained at 36 °C. Penetration of microelectrodes filled with 3 M KCl (resistance, 20 to 50 MΩ) was made into dominant pacemaker cells. The output of the microelectrode amplifier (MEZ-8201, Nihon Kohden, Tokyo, Japan) was fed into an AD converter (Analog Pro, Canopus, Kobe, Japan) attached to a computer (PC 9801 FA2, NEC, Tokyo, Japan) for the analyses. The parameters measured were cycle length, maximum diastolic potential, slope of the diastolic depolarization (slope), threshold potential, maximum rate of rise of the upstroke of the action potential (maximum rate of rise), overshoot, and duration at 50% repolarization. The effect of efonidipine on the action potential in myocardial tissue preparations is known to be slow in onset and requires higher concentrations than its effects on calcium currents in single cells (Okuyama et al., 1994; Masuda et al., 1995; Tanaka et al., 1996; Masumiya et al., 1998). To measure the effect of drugs on the action potential accurately, we used a single relatively high concentration of drugs (1 μM). The exposure time was 2 min for nifedipine but was 30 min for efonidipine, which required longer time for its effect to reach steady state. For the interpretation of results, the effect of the two enantiomers of efonidipine might have to be compared with their effects on the calcium currents at lower concentrations.

2.2. Expression and analysis of $Ca_V1.2$ and $Ca_V1.3$

Expression of calcium channel α-subunits $Ca_V1.2$, $Ca_V1.3$ in BHK6 cells and current measurement were performed as previously described (Yamaguchi et al., 2000). The cDNA for $Ca_V1.2$ and $Ca_V1.3$ were generously provided by Dr. Snutch, T.P. (British Columbia University, Canada) and Striessnig, J. (University of Innsbruck, Austria), respectively. The full length cDNAs for $Ca_V1.2$ and $Ca_V1.3$ were introduced into BHK6 cells expressing the calcium channel β_{1a} and α_2/δ subunits. We confirmed that $Ca_V1.3$ activated at more negative voltages compared to $Ca_V1.2$ by approximately 20 mV, as has been reported (Koschak et al., 2001). Therefore, inward currents through $Ca_V1.2$ and $Ca_V1.3$ channels were elicited by 100 ms depolarizing voltage clamp pulses from −80 mV to 10 mV and −10 mV, respectively. The extracellular solution was of the following composition (mM concentration): NaCl, 137.0; KCl, 5.4; $BaCl_2$, 10; $MgCl_2$, 1; glucose, 10; tetrodotoxin 0.0001; HEPES, 10 (pH 7.4) and the pipette solution was of the following composition (mM concentration): cesium methanesulfonate, 120; tetraethylammoniumCl, 20; EGTA, 14; ATP-Mg, 5; Na_2GTP, 0.2;Na_2 creatine phosphate, 5; HEPES, 10 (pH 7.3). The charge carrier for the calcium channel currents was Ba^{2+} instead of Ca^{2+}. The output of the patch clamp amplifier (HEKA Elektonik, Lambrecht Germany) was digitalized with an AD converter (Digidata 1322A, Axon Instruments Inc., Foster City USA) and analyzed (pClamp-9 software, Axon Instruments Inc., Foster City USA). The exposure time of the drugs on the calcium channel currents was 10 min, during which the current rundown was less than 5%.

2.3. Expression and analysis of $Ca_V3.1$

The full length cDNA for $Ca_V3.1$ was obtained by polymerase chain reaction from a mouse heart cDNA library (Takara Bio Co., Ltd., Kyoto, Japan) according to the published mouse cDNA sequence (Klugbauer et al., 1999; GenBank accession number AJ012569), and inserted into the mammalian expression vector pIRESneo3 (Takara Bio Co., Ltd., Kyoto, Japan). This vector was introduced into HEK293 cells with lipofectamine 2000 (Invitrogen, Carlsbad CA, USA) and stable transformants were obtained by clone culture in the presence of 500 μM G418. Inward currents through the $Ca_V3.1$ channels were elicited by 200 ms depolarizing voltage clamp pulses from −80 mV to −30 mV, as described previously (Tanaka et al., 2008). The extracellular solution was of the following composition (mM concentration): NaCl, 143.0; KCl, 5.4; $CaCl_2$, 1.8; $MgCl_2$, 1.0; KH_2PO_4, 0.33; HEPES, 5.0; and glucose, 5.5 (pH 7.4). The pipette solution was of the following composition (mM concentration): CsCl, 80; CsOH, 40; ATP-Mg, 5; EGTA, 10; and HEPES, 10 (pH 7.2). The patch clamp amplifier used was Axopatch 1D (Axon Instruments Inc., Foster City CA, USA) and the AD converter was Digidata 1200 (Axon Instruments Inc., Foster City CA, USA). The exposure time of the drugs on the calcium channel currents was 10 min, during which the current rundown was less than 5%.

2.4. Data analysis and statistics

Data were presented as mean ± standard errors (S.E.M.). Statistical significance between means was evaluated by the paired t-test or by one-way analysis of variance followed by Dunnett's test for multiple comparisons. P values less than 0.05 were considered significant.

2.5. Drugs and chemicals

The enantiomers of efonidipine {5-(5,5-Dimethyl-1,3,2-dioxaphosphorinan-2-yl)-1,4-dihydro-2,6-dimethyl-4-(3-nitrophenyl)-3-pyridinecarboxylic acid 2-[phenyl(phenylmethyl)amino]ethyl ester} were provided by Nissan Chemical Industries, Ltd. (Tokyo, Japan), and nifedipine was purchased from Wako Pure Chemical Industries, Ltd. (Osaka, Japan). The drugs were dissolved in DMSO and small aliquots were applied to the extracellular solution; the final concentration of DMSO was 0.05%. All other chemicals were commercial products of the highest available quality.

3. Results

3.1. Effect of S(+)-efonidipine, nifedipine and R(−)-efonidipine on sinus node action potential

The effect of S(+)-efonidipine on sinus node action potential was examined and compared with those of nifedipine and R(−)-efonidipine (Fig. 1; Table 1). S(+)-Efonidipine (1 μM) significantly reduced the slope of phase 4 and phase 0 depolarization. Nifedipine (1 μM) also significantly reduced the slope of phase 0 depolarization but only slightly reduced the slope of phase 4 depolarization. R(−)-efonidipine (1 μM) had no significant effect on these parameters. S(+)-efonidipine and nifedipine prolonged the cycle length and shifted the maximum diastolic potential and the threshold potential towards depolarized potentials but such effects were not observed with R(−)-efonidipine.

3.2. Effect of S(+)-efonidipine on calcium channel currents

The effect of S(+)-efonidipine on calcium channel α-subunits $Ca_V1.2$, $Ca_V1.3$ and $Ca_V3.1$ were compared with those of nifedipine and R(−)-efonidipine. S(+)-Efonidipine inhibited the expressed $Ca_V1.2$, $Ca_V1.3$ and $Ca_V3.1$ channel currents with similar potency (Fig. 2Aabc; 2Ba). The effect was concentration-dependent and the percent inhibition of $Ca_V1.2$, $Ca_V1.3$ and $Ca_V3.1$ currents by 1 μM S(+)-efonidipine was 75.7%, 75.3% and 94.0%, respectively, and the EC_{50} value was 0.46 μM, 0.32 μM and 0.11 μM, respectively.

3.3. Effect of nifedipine on calcium channel currents

Nifedipine inhibited the expressed $Ca_V1.2$, $Ca_V1.3$ and $Ca_V3.1$ channel currents; the effect was concentration-dependent and the potency order was $CaV1.2 > Ca_V1.3 > Ca_V3.1$ (Fig. 2Adef; 2Bb). Percent inhibition of $Ca_V1.2$, $Ca_V1.3$ and $Ca_V3.1$ currents by 1 μM nifedipine was 84.0%, 43.2% and 14.9%, respectively, and the EC_{50} value for the $Ca_V1.2$ and $Ca_V1.3$ channel currents was 0.19 μM and 2.82 μM, respectively.

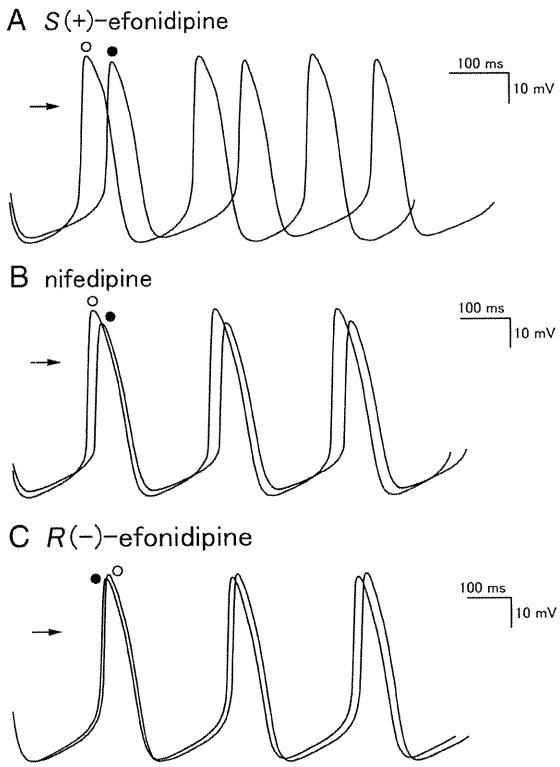

Fig. 1. Effects of *S*(+)-efonidipine, nifedipine and *R*(−)-efonidipine on rabbit sinus node action potential. Typical recordings before (open circles) and after (closed circles) the addition of 1 μM *S*(+)-efonidipine (A), 1 μM nifedipine (B) and 1 μM *R*(−)-efonidipine (C). Arrows indicate 0 mV level.

3.4. Effect of *R*(−)-efonidipine on calcium channel currents

R(−)-Efonidipine inhibited the expressed $Ca_V1.2$, $Ca_V1.3$ and $Ca_V3.1$ channel currents; the effect was concentration-dependent and the potency order was $Ca_V3.1 > Ca_V1.2 = Ca_V1.3$ (Fig. 2Bc). Percent inhibition of $Ca_V1.2$, $Ca_V1.3$ and $Ca_V3.1$ currents by 1 μM *R*(−)-efonidipine was 30.0%, 19.6% and 92.8%, respectively, and the EC_{50} value for the $Ca_V3.1$ channel current was 0.20 μM.

4. Discussion

4.1. Prolongation of the phase 4 depolarization of sinus node action potential

The main objective of the present study was to determine whether the effect of efonidipine to prolong the phase 4 depolarization of the sinus node originates in the *S*(+)-enantiomer. In the rabbit sinus node, *S*(+)-efonidipine significantly reduced the slope of phase 4 depolarization (Fig. 1A), which was the same as the effect of racemic efonidipine (Masumiya et al., 1997); such effect was not observed with *R*(−)-efonidipine (Fig. 1C). These results clearly indicate that prolongation of the phase 4 depolarization of rabbit sinus node is caused by the *S*(+)-enantiomer. Thus, clarification of the mechanism of action of *S*(+)-efonidipine may lead to a new understanding of pacemaker mechanisms. *S*(+)-efonidipine and nifedipine caused a slight positive shift of the maximum diastolic potential. As the inhibitory effect of efonidipine and nifedipine on the inwardly rectifying and delayed rectifying potassium currents are minimal (Masumiya et al., 1998), and efonidipine had no effect on the hyperpolarization-activated inward current (unpublished observation), effects on other ionic currents and/or indirect mechanisms may be involved.

4.2. Possible mechanism for the prolongation of phase 4 depolarization

S(+)-efonidipine blocked all three calcium channel α subunits $Ca_V1.2$, $Ca_V1.3$ and $Ca_V3.1$ with similar potency (Fig. 2Ba), EC_{50} values being 0.46, 0.32 and 0.11 (μM), respectively. To obtain information on the mechanism of action for the prolongation of phase 4 depolarization by *S*(+)-efonidipine, the effects were compared with those of nifedipine and *R*(−)-efonidipine. Nifedipine, which blocked the $Ca_V1.2$ and $Ca_V1.3$ channel currents with EC_{50} values of 0.19 and 2.28 (μM), respectively (Fig. 2Bb), produced a less prominent prolongation of phase 4 depolarization (Fig. 1B). *R*(−)-efonidipine, which was selective for the $Ca_V3.1$ channel (Fig. 2Bc), had no prolonging effect on phase 4 depolarization (Fig. 1C). This parallelism of potency of the three compounds to block the $Ca_V1.3$ channel and to prolong the phase 4 depolarization suggests a causal relationship; the $Ca_V1.3$ channel current contributes to phase 4 depolarization. The $Ca_V1.3$ channel may be a novel target molecule for the development of bradycardiac agents. The activation threshold for the $Ca_V1.2$ channel is

Table 1
Action potential parameters before and after application of *S*(+)-efonidipine, nifedipine, *R*(−)-efonidipine and their vehicle.

	S(+)-efonidipine (n = 5)		nifedipine (n = 5)		*R*(−)-efonidipine (n = 5)		vehicle (DMSO) (n = 5)	
	before	after	before	after	before	after	before	after
Cycle length (ms)	296 ± 27	322 ± 26[a] (26 ± 7)[b]	304 ± 15	314 ± 15[a] (11 ± 1)	325 ± 37	318 ± 33 (−7 ± 5)	316 ± 19	312 ± 21 (−3 ± 3)
Maximum diastolic potential (mV)	−60.5 ± 0.3	−56.6 ± 0.8[a] (4.0 ± 0.8)	−61.0 ± 2.0	−58.7 ± 2.2[a] (2.4 ± 0.4)	−59.8 ± 0.8	−57.1 ± 1.6 (2.7 ± 1.5)	−59.6 ± 3.0	−58.2 ± 2.7 (1.4 ± 0.6)
Slope (mV/s)	89.1 ± 11.1	71.3 ± 7.3[a] (−17.8 ± 5.8)[b]	90.1 ± 5.1	82.0 ± 3.4 (−8.1 ± 4.9)	79.8 ± 12.1	78.3 ± 13.1 (−1.5 ± 1.9)	88.3 ± 6.7	89.3 ± 6.8 (1.0 ± 1.0)
Threshold potential (mV)	−47.9 ± 1.4	−43.2 ± 0.8[a] (4.7 ± 1.0)	−47.6 ± 2.0	−45.8 ± 1.8[a] (1.8 ± 0.4)	−38.1 ± 3.0	−36.4 ± 2.4 (2.8 ± 1.8)	−45.7 ± 2.9	−44.0 ± 2.7 (1.7 ± 0.7)
Maximum rate of rise (V/s)	13.2 ± 2.3	10.3 ± 2.4[a] (−2.9 ± 0.6)	14.2 ± 2.7	11.2 ± 1.9[a] (−2.9 ± 0.9)	14.4 ± 3.1	12.1 ± 2.6 (−2.3 ± 0.9)	10.7 ± 1.6	9.7 ± 1.5 (−1.0 ± 0.6)
Overshoot (mV)	20.6 ± 2.5	17.3 ± 4.3 (−3.3 ± 2.0)	17.7 ± 2.2	14.4 ± 2.3[a] (−3.3 ± 0.3)	21.1 ± 2.5	20.2 ± 2.6 (−1.0 ± 0.5)	22.0 ± 1.5	22.5 ± 1.7 (0.4 ± 0.3)
Duration at 50% repolarization (ms)	60.6 ± 3.5	56.5 ± 4.1[a] (−4.2 ± 0.8)[b]	67.1 ± 6.0	62.5 ± 5.7[a] (−4.6 ± 0.8)[b]	69.5 ± 2.7	68.1 ± 2.9[a] (−1.4 ± 0.4)	68.5 ± 6.0	67.8 ± 6.0 (−0.7 ± 0.4)

Slope indicates the slope of the phase 4 depolarization and maximum rate of rise indicates the maximum slope of the action potential upstroke (phase 0). After: 30 min after the application of 1 μM *S*(+)-efonidipine and *R*(−)-efonidipine and vehicle (0.05% DMSO), 2 min after the application of 1 μM nifedipine. The changes in parameters are indicated in parenthesis.
[a] Significant difference from corresponding values before the application of drugs as evaluated by the paired t-test.
[b] Significant difference from corresponding changes after vehicle application as evaluated by Dunnett's test for multiple comparisons.

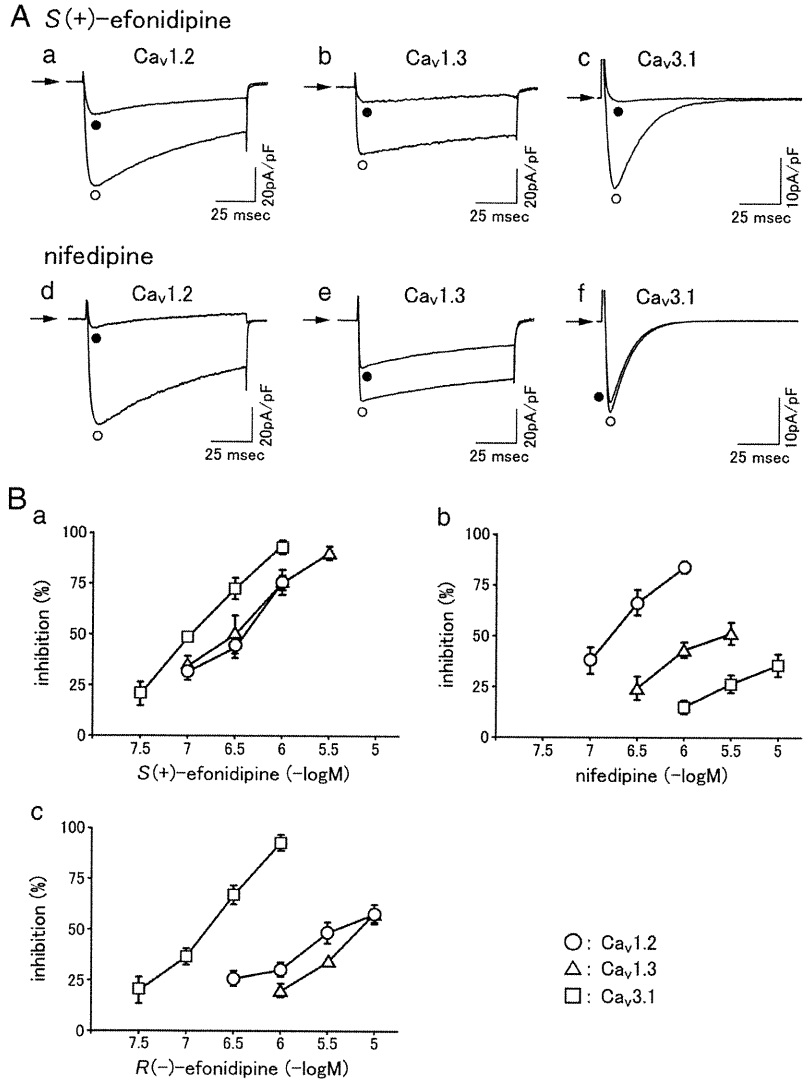

Fig. 2. Effects of *S*(+)-efonidipine, nifedipine and *R*(−)-efonidipine on calcium channel α-subunits $Ca_V1.2$, $Ca_V1.3$ and $Ca_V3.1$. A: Typical current recordings before (open circles) and after (closed circles) the addition of 1 μM *S*(+)-efonidipine on $Ca_V1.2$ (a), $Ca_V1.3$ (b) and $Ca_V3.1$ (c) channel currents and 1 μM nifedipine on $Ca_V1.2$ (d), $Ca_V1.3$ (e) and $Ca_V3.1$ (f) channel currents. Arrows indicate zero current level. B: Concentration–response relationship for the effects of *S*(+)-efonidipine (a), nifedipine (b) and *R*(−)-efonidipine (c) on calcium channel α-subunits $Ca_V1.2$ (circles), $Ca_V1.3$ (triangles) and $Ca_V3.1$ (squares). Symbols and vertical bars indicate the mean ± standard error of the mean from five to eight experiments.

about −30 mV (Koschak et al., 2001), which is more positive than the threshold potential (takeoff potential) of the sinus node action potential. Thus, the inhibitory effect of S(+)-efonidipine and nifedipine on the $Ca_V1.2$ channel current can be the cause of the decrease in maximum rate of rise, but not of the decreases in the slope and threshold potential (Table 1). Concerning the $Ca_V3.1$ channel current (T-type calcium current), we have previously reported that *R*(−)-efonidipine prolongs the phase 4 depolarization of the sinus node action potential in the mouse and guinea-pig but not in the rabbit (Tanaka et al., 2008). This agrees with the view that, under normal conditions, the T-type calcium current contributes to phase 4 depolarization in smaller animals such as the mouse and guinea-pig, but not in larger animals such as the rabbit and pig (Ono and Iijima, 2005).

4.3. Contribution of the $Ca_V1.3$ channel current to phase 4 depolarization

Contribution of the $Ca_V1.3$ channel current to the phase 4 depolarization of the sinus node action potential is consistent with the reported electrophysiological properties of the $Ca_V1.3$ channel. The $Ca_V1.3$ channel was reported to have an activation range of −50 mV to −10 mV, the voltage for 5% activation being −46 mV (Koschak et al., 2001). These values were about 20 mV negative than those for $Ca_V1.2$. This means that the $Ca_V1.3$ channel current can contribute to the phase 4 depolarization of the sinus node which occurs at −60 to −40 mV. This does not necessarily exclude the contribution of other membrane currents to phase 4 depolarization. In fact, the reduction of the slope by *S*(+)-efonidipine was partial which indicates that *S* (+)-efonidipine-insensitive mechanisms also contribute to the phase 4 depolarization of the rabbit sinus node.

5. Conclusion

The present results indicated that *S*(+)-efonidipine is responsible for the prolongation by racemic efonidipine of the phase 4 depolarization of the rabbit sinus node, and provided pharmacological evidence that the $Ca_V1.3$ channel current contributes to the phase 4 depolarization of the sinus node action potential.

Acknowledgments

This study was partly performed as a part of the project "Research on the molecular mechanisms of appearance of age-related diseases by failure of cell function control system, and their prevention and treatment" by the "Research Center for Aging and Age-Related Diseases" established in the Toho University Faculty of Pharmaceutical Sciences. This study was supported in part by Grants-in-Aid from the Ministry of Education, Culture, Sports, Science, and Technology of Japan to I.N (#22790262), A.T. (#21590602), and H.T.(#21590293) and by The Pharmacological Research Foundation, Tokyo. This study was supported in part by a research grant for collaborative research project in Toho University.

References

Furukawa, T., Miura, R., Honda, M., Kamiya, N., Mori, Y., Takeshita, S., Isshiki, T., Nukada, T., 2004. Identification of *R*-(−)-isomer of efonidipine as a selective blocker of T-type Ca^{2+} channels. Br. J. Pharmacol. 143, 1050–1057.

Klugbauer, N., Marais, E., Lacinova, L., Hofmann, F., 1999. A T-type calcium channel from mouse brain. Pflugers Arch. Eur. J. Physiol. 437, 710–715.

Koschak, A., Reimer, D., Huber, I., Grabner, M., Glossmann, H., Engel, J., Striessnig, J., 2001. α1D ($Ca_V1.3$) subunits can form L-type Ca^{2+} channels activating at negative voltages. J Biol Chem 276, 22100–22106.

Mangoni, M.E., Couette, B., Bourinet, E., Platzer, J., Reimer, D., Striessnig, J., Nargeot, J., 2003. Functional role of L-type $Ca_V1.3$ Ca^{2+} channels in cardiac pacemaker activity. Proc. Natl. Acad. Sci. USA 100, 5543–5548.

Masuda, Y., Tanaka, S., 1994. Efonidipine hydrochloride: a new calcium antagonist. Cardiovasc. Drug Rev. 12, 123–135.

Masuda, Y., Miyajima, M., Shudo, C., Tanaka, S., Shigenobu, K., Kasuya, Y., 1995. Cardiovascular selectivity of 1, 4-dihydropyridine derivatives, efonidipine (NZ-105), nicardipine and structure related compounds in isolated guinea-pig tissues. Gen. Pharmacol. 26, 339–345.

Masumiya, H., Tanaka, H., Shigenobu, K., 1997. Effects of Ca^{2+} channel antagonists on sinus node: prolongation of late phase 4 depolarization by efonidipine. Eur. J. Pharmacol. 335, 15–21.

Masumiya, H., Shijyuku, T., Tanaka, H., Shigenobu, K., 1998. Inhibition of myocardial T- and L-type Ca^{2+} currents by efonidipine: possible mechanism for its chronotropic effect. Eur. J. Pharmacol. 349, 351–357.

Morimoto, S., Jo, T., Maki, K., Iwasaka, T., 2009. Effects of efonidipine hydrochloride on heart rate and circulatory changes due to stress. Clin. Exp. Hypertens. 31, 83–91.

Ohashi, N., Mitamura, H., Ogawa, S., 2009. Development of newer calcium channel antagonists: therapeutic potential of efonidipine in preventing electrical remodeling during atrial fibrillation. Drugs 69, 21–30.

Okuyama, R., Adachi-Akahane, S., Nagao, T., 1994. Differential potentiation by depolarization of the effects of calcium antagonists on contraction and Ca^{2+} current in guinea-pig heart. Br. J. Pharmacol. 113, 451–456.

Ono, K., Iijima, T., 2005. Ionic and molecular basis of cardiac automaticity in mammalian heart. In: Mizukami, Y., Ohtsuka, T. (Eds.), Molecular mechanisms of heart diseases. Research SignPost, Trivandrum, pp. 1–22.

Platzer, J., Engel, J., Schrott-Fischer, A., Stephan, K., Bova, S., Chen, H., Zheng, H., Striessnig, J., 2000. Congenital deafness and sinoatrial node dysfunction in mice lacking class D L-type Ca^{2+} channels. Cell 102, 89–97.

Shimizu, M., Ogawa, K., Sasaki, H., Mizokami, T., Uehara, Y., Mochizuki, S., 2001. Effect of efonidipine hydrochloride, dihydropyridine Ca^{2+} antagonist with T-type Ca^{2+} channel blocking action, on heart rate. Ther. Res. 22, 883–889.

Tanaka, H., Shigenobu, K., 2002. Efonidipine hydrochloride: a dual blocker of L- and T-type Ca^{2+} channels. Cardiovasc. Drug Rev. 20, 81–92.

Tanaka, H., Shigenobu, K., 2005. Pathophysiological significance of T-type Ca^{2+} channels: T-type Ca^{2+} channels and drug development. J. Pharmacol. Sci. 99, 214–220.

Tanaka, H., Masumiya, H., Sekine, T., Shijuku, T., Sugahara, M., Taniguchi, H., Terada, M., Saito, W., Shigenobu, K., 1996. Myocardial and vascular effects of efonidipine in vitro as compared with nifedipine, verapamil and diltiazem. Gen. Pharmacol. 27, 451–454.

Tanaka, H., Komikado, C., Shimada, H., Takeda, K., Namekata, I., Kawanishi, T., Shigenobu, K., 2004. The *R*(−)-enantiomer of efonidipine blocks T-type but not L-type calcium current in guinea pig ventricular myocardium. J. Pharmacol. Sci. 96, 499–501.

Tanaka, H., Komikado, C., Namekata, I., Nakamura, H., Suzuki, M., Tsuneoka, Y., Shigenobu, K., Takahara, A., 2008. Species difference in the contribution of T-type calcium current to cardiac pacemaking as revealed by *R*(−)-efonidipine. J. Pharmacol. Sci. 107, 99–102.

Tanaka, T., Tsutamoto, T., Sakai, H., Fujii, M., Yamamoto, T., Horie, M., 2007. Comparison of the effects of efonidipine and amlodipine on aldosterone in patients with hypertension. Hypertens. Res. 30, 691–697.

Yamaguchi, S., Okamura, Y., Nagao, T., Adachi-Akahane, S., 2000. Serine residue in the IIIS5-S6 linker of the L-type Ca^{2+} channel α_{1c} subunit is the critical determinant of the action of dihydropyridine Ca^{2+} channel agonists. J. Biol. Chem. 275, 41504–41511.

Zhang, Z., Zu, Y., Song, H., Rodriguez, J., Tuteja, D., Namkung, Y., Shin, H., Chiamvimonvat, N., 2002. Functional roles of $Ca_V1.3$ ($\alpha1_D$) calcium channel in sinoatrial nodes. Insight gained using gene-targeted null mutant mice. Circ. Res. 90, 981–987.

Effect of NIP-142 on Potassium Channel α-Subunits Kv1.5, Kv4.2 and Kv4.3, and Mouse Atrial Repolarization

Hikaru TANAKA,*[,a] Iyuki NAMEKATA,[a] Shogo HAMAGUCHI,[a] Taro KAWAMURA,[a] Hiroyuki MASUDA,[a] Yoshio TANAKA,[a,b] Naoko IIDA-TANAKA,[a,c] and Akira TAKAHARA[a]

[a] *Department of Pharmacology, Toho University Faculty of Pharmaceutical Sciences;* [b] *Department of Chemical Pharmacology, Toho University Faculty of Pharmaceutical Sciences; Funabashi, Chiba 274–8510, Japan; and* [c] *Department of Food Science, Otsuma Woman's University; Chiyoda-ku, Tokyo 102–8357, Japan.*
Received July 25, 2009; accepted October 21, 2009; published online October 22, 2009

Effects of NIP-142, a benzopyran compound which terminates experimental atrial arrhythmia, on potassium channel α-subunits and mouse atrial repolarization were examined. NIP-142 concentration-dependently blocked the outward current through potassium channel α subunits Kv1.5, Kv4.2 and Kv4.3 expressed in *Xenopus* oocytes. In isolated mouse atrial myocardia, NIP-142 prolonged the action potential duration and effective refractory period, and increased the contractile force. These results suggest that NIP-142 blocks the potassium channels underlying the transient and sustained outward currents, which may contribute to its antiarrhythmic activity.

Key words NIP-142; Kv1.5; Kv4.2; Kv4.3; atrial fibrillation

Atrial fibrillation is one of the most frequent types of arrhythmia and is reported to double the risk of deaths due to cardiovascular diseases. It is also the major risk factor for thromboembolism, especially cerebral embolism.[1] At present, atrial fibrillation is mainly treated with class I antiarrhythmic agents such as pilsicainide and flecainide, or class III antiarrhythmic agents such as dofetilide and amiodarone.[2—4] However, the major problem with these agents is that they also affect ventricular excitation and repolarization. Thus, drugs with atrial selectivity are desired for the treatment of atrial fibrillation.

NIP-142, (3*R**,4*S**)-4-cyclopropylamino-3,4-dihydro-2,2-dimethyl-6-(4-methoxyphenylacethylamino)-7-nitro-2*H*-1-benzopyran-3-ol, is a benzopyran derivative with terminating effects on canine vagal stimulation-induced atrial fibrillation model and on canine Y-shaped incision-induced atrial flutter model.[5] These effects have been attributed to prolongation of atrial refractory period. The prolongation of the refractory period and action potential duration (APD) by NIP-142 was observed in the atrium,[5,6] but not in the ventricle.[6] This may indicate that NIP-142 is less likely to disturb ventricular repolarization when applied for the treatment of atrial arrhythmia. In isolated human atrial cardiomyocytes, NIP-141, the hydrochloride salt of NIP-142, concentration-dependently inhibited the transient and sustained components of the outward current.[7] However, the molecular identity of the ion channels subject to inhibition has not yet been clarified. In the present study, we examined the effect of NIP-142 on expressed potassium channel α subunits Kv1.5, Kv4.2 and Kv4.3, which underlie the transient and sustained outward currents. As inhibitory effects were observed on these currents, we also examined the effect of NIP-142 on action potential duration, effective refractory period and contractile force in isolated mouse atrial myocardium. The effects of NIP-142 were compared with those of 4-aminopyridine to obtain information on the mechanism of action of NIP-142.

MATERIALS AND METHODS

Cloning of Mouse Kv1.5, Kv4.2 and Kv4.3 cDNA and Preparation of Specific cRNAs cDNA fragments for Kv1.5, Kv4.2 and Kv4.3 were amplified by polymerase chain reaction from a mouse heart cDNA library (Takara Shuzo Co., Ltd., Kyoto, Japan) with oligonucleotide primers designed based on the published mouse cDNA sequence of Kv1.5 (GenBank accession number AF108659), Kv4.2 (AF107780) and Kv4.3L (AF107781). The nucleotide sequence of the primers used for Kv1.5 were 5′-ATGCCCCTTGCCCCCGGGCCATGG-3′, 5′-GCTCTGCCAGCTCGGTGCCCAGGG-3′, 5′-TTTCTTTGCTTGCCCCAGCAAGGC-3′ and 5′-CAAGTCTGCCTCGATCTCTCTTTAC-3′, those for Kv4.2 were 5′-CAGACAACATGGCAGCCGGTGTTG-3′, 5′-AAGACTCCGCTCAGTGAGCAGATG-3′, 5′-AGCAAGCAAGTTCACCAGCATCCC-3′ and 5′-GCTCTCAGACCTGTGCCAATTGTC-3′, and those for Kv4.3 were 5′-CTGGAGTCACCATGGCGGCAGGAGTTG-3′, 5′-GGATGCTTGTGAACTTGCTGGCAG-3′, 5′-TGACCAACAATGAGGACGTGTCTG-3′ and 5′-CCCCCTCAGGCCCTCTGTCCAGTG-3′. These cDNA fragments were assembled with standard ligation techniques, and the full length cDNAs were separately inserted into the pGEM11Zf vector (Promega, Madison, WI, U.S.A.). The cRNAs for Kv1.5, Kv4.2 and Kv4.3 were obtained by *in vitro* transcription from linearized plasmid templates with mMESSAGE mMACHINE *in vitro* Transcription T7 kit (Ambion, Inc., Austin, TX, U.S.A.).

Oocyte Culture and Electrophysiological Assay *Xenopus laevis* oocytes were isolated from ovary lobes by collagenase treatment as described.[8] Then the oocytes were injected with cRNAs for Kv1.5, Kv4.2 or Kv4.3 (10 ng of each cRNA per oocyte) and were further incubated for 2—4 d until the electrophysiological assay. Two-electrode voltage clamp was performed as described[8] with OC-725 amplifier (Warner Instruments, Inc., Hamden, CT, U.S.A.) and glass microelectrodes filled with 3M KCl (0.5 to 2.0 MW). Oocytes were placed in a recording chamber perfused with ND96 solution

* To whom correspondence should be addressed. e-mail: htanaka@phar.toho-u.ac.jp

supplemented with $CaCl_2$ (composition in mM: NaCl 96, KCl 2, $MgCl_2$ 1, $CaCl_2$ 1.8, *N*-(2-hydroxyethyl)piperazine-*N'*-2-ethanesulfonic acid (HEPES) 5, pH 7.5). All experiments were performed at room temperature. Data acquisition and analysis were performed with pClamp software (Axon Institute).

Experiments with Isolated Mouse Atria All experiments with the mouse were approved by the Ethics Committee of Toho University, and were performed in accordance with the "Guiding Principles for the Care and Use of Laboratory Animals" approved by the Japanese Pharmacological Society. The left atria were isolated from ddy mice and measurement of the action potential with standard glass microelectrode techniques and measurement of contractile force were performed as described.[9] Measurement of the effective refractory period was performed by extracellular recording as previously described.[6]

Drugs and Chemicals NIP-142 was synthesized by Nissan Chemical Industries (Tokyo, Japan). NIP-142 was added to the bath solution from a stock solution (100 mM) in 0.1 M HCl. The final concentration of HCl in the measuring bath (<0.1 mM) did not affect any of the experimental parameters measured. All other chemicals were commercial products of the highest available grade of quality.

Statistical Analysis All experimental data are expressed as mean±standard errors of the mean (S.E.M.). The statistical significance of differences between means was evaluated by the paired *t*-test or the Dunnet's test for multiple comparisons as appropriate. A value of $p<0.05$ was considered statistically significant.

RESULTS

In *Xenopus* oocytes injected with the cRNAs for Kv1.5, Kv4.2 and Kv4.3, depolarization to membrane potentials more positive than −30 mV from a holding potential of −80 mV evoked outward currents. The Kv1.5 current showed rapid activation and very slow inactivation (Fig. 1A). The Kv4.2 and Kv4.3 currents showed rapid activation and inactivation (Figs. 1B, C). NIP-142, 10 μM and 100 μM, inhibited these outward currents both at the outward current peak and at the end of the 200 ms depolarizing pulse. The inhibition was concentration-dependent and statistically significant (Fig. 1D). The inhibition by 100 μM was larger with the Kv1.5 current. 4-Aminopyridine also inhibited these currents. At 100 μM, inhibition was observed only for the Kv1.5 channel current; the early phase outward current at 30 ms depolarization was reduced to 65.0±1.5% ($n=5$). At 1 mM, the Kv1.5, Kv4.2 and Kv4.3 channel currents (early phase or peak outward) were reduced to 12.4±3.2%, 85.0±3.1% and 92.8±2.7%, respectively ($n=5$). At 10 mM, all of these currents were completely inhibited.

The isolated mouse left atria had an action potential with short duration. 4-Aminopyridine induced a prolongation of the early phase repolarization (Fig. 2A) while tertiapin induced prolongation of the late phase (Fig. 2B). NIP-142 prolonged both the early and late phases of repolarization (Fig. 2C); the effect was concentration-dependent (Table 1). NIP-

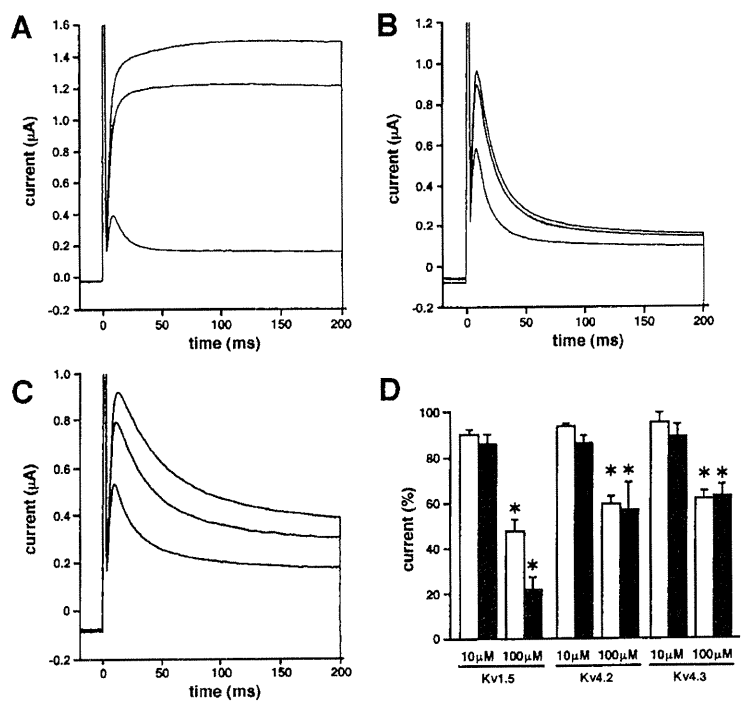

Fig. 1. Effect of NIP-142 on Potassium Channel Currents Expressed in *Xenopus* Oocytes

Typical current recordings for Kv1.5 (A), Kv4.2 (B), Kv4.3 (C) during 200 ms depolarizing voltage clamp pulses from −80 to +40 mV in the absence and presence of 10 μM and 100 μM NIP-142. Summarized results are shown in D. Columns and vertical bars indicate the mean±S.E.M. from 3 experiments. Open columns indicate the effects on the early phase (30 ms after depolarization for Kv1.5 and at the outward current peak for Kv4.2 and 4.3) and closed columns indicate those on the sustained current at the end of the depolarizing pulse. Asterisks indicate significant difference ($p<0.05$) from corresponding values before the application of NIP-142 as determined by the Dunnet's test for multiple comparisons.

Table 1. Effect of 4-Aminopyridine, Tertiapin and NIP-142 on Mouse Atrial Action Potential Duration

		4-Aminopyridine (1 mM)	4-Aminopyridine (10 mM)	Tertiapin (1 μM)	NIP-142 (1 μM)	NIP-142 (10 μM)	NIP-142 (100 μM)
APD_{20} (ms)	Before	3.3±0.4	4.4±0.3	2.4±0.2	2.7±0.4	2.6±0.1	2.7±0.2
	After	8.5±0.4*	18.6±1.3*	2.5±0.3	2.6±0.3	3.5±0.2*	12.7±2.1*
APD_{90} (ms)	Before	32.8±2.2	36.2±2.1	39.1±2.9	33.2±3.7	33.0±2.9	35.0±2.3
	After	32.8±1.9	60.0±3.1*	59.8±3.8*	34.7±4.0	44.9±1.5*	90.5±6.3*

Action potential duration at 20% repolarization (APD_{20}) and 90% repolarization (APD_{90}) were measured before and 30 min after the addition of 1 mM or 10 mM 4-aminopyridine, 1 μM tertiapin, and 1 to 100 μM NIP-142. Values indicate the mean±S.E.M. from 4 to 5 experiments. Asterisks on values after addition indicate significant difference ($p<0.05$) from corresponding values before addition as determined by the paired t-test.

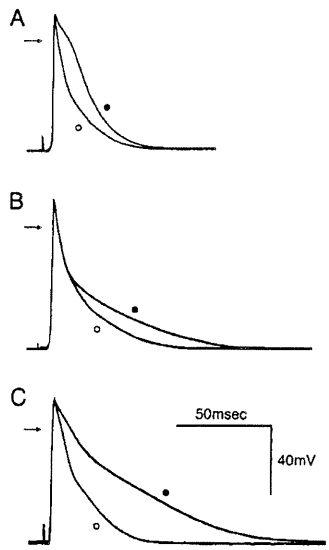

Fig. 2. Effect of 4-Aminopyridine, Tertiapin and NIP-142 on Mouse Atrial Action Potential

Typical action potential records obtained in the absence (open circles) and presence (closed circles) of 1 mM 4-aminopyridine (A), 1 μM tertiapin (B) and 100 μM NIP-142 (C). Arrows indicate zero mV level.

142 (100 μM) prolonged the effective refractory period of isolated mouse atria from 43.0±2.6 ms to 71.0±5.1 ms ($n=5$); the increase was statistically significant. 4-Aminopyridine, 1 mM and 10 mM, increased the contractile force from 122.3±25.9 mg to 219.3±42.6 mg (184%) and 359.5±50.3 mg (319%), respectively ($n=5$); the increases were statistically significant.

DISCUSSION

NIP-142 concentration-dependently blocked the Kv1.5, Kv4.2 and Kv4.3 potassium channel currents (Fig. 1). These currents are considered to be the major repolarizing currents in the rodent myocardium and also to contribute to repolarization in the myocardium of many species including human. NIP-142 was shown to block the repolarizing outward currents in human atrial cardiomyocytes, but the molecular target of the blocking effect had not been clarified.[7] The present results show that NIP-142 blocks the Kv1.5, Kv4.2 and Kv4.3 channel currents (Fig. 1), the inhibitory effect of 100 μM NIP-142 on Kv1.5 was larger than that on Kv4.2 and Kv4.3. We have previously reported the inhibitory action of NIP-142 on human Kv1.5.[10] The potency of NIP-142 on human Kv1.5 was slightly higher than in the present study with mouse Kv1.5, which may reflect species difference in the structure of the Kv1.5 channel. Alternatively, the difference in potency may be due to the difference in expression systems; human Kv1.5 in our previous study was expressed in HEK293 cells, which is generally known to result in higher sensitivity of expressed ion channel to inhibitory agents compared with the *Xenopus* oocyte system.

The mRNAs for Kv1.5, Kv4.2 and Kv4.3, which underlie the transient outward current, is detected both in human[11] and mouse atria.[12] The mouse atrium has a larger transient outward current-density[7,12] and shorter action potential duration[12,13] than the human atrium. Prolongation by 1 mM and 10 mM 4-aminopyridine of the early repolarization phase of the mouse atrial action potential (Table 1; Fig. 1A) indicates that the transient outward current through Kv1.5, Kv4.2 and Kv4.3 channels is the major determinant of early repolarization.[14] Thus, the mouse atrial myocardium provides an experimental model to study the effect of agents modifying these channels.[15] NIP-142 was shown to prolong the early phase repolarization indicating that it indeed blocks the transient outward current in the atrial cardiomyocyte. The late repolarization, on the other hand, appears to be influenced by currents dominating in the voltage range more negative than −40 mV including the acetylcholine-activated potassium current. In guinea-pig myocardium, we have shown that the acetylcholine-activated potassium current is present in the atrial myocardium in the absence of muscarinic receptor stimulation, and that NIP-142 prolongs action potential duration and effective refractory period through blockade of this current.[6,8] Such effect was not observed in the ventricle which may explain the atria-selective nature of NIP-142. Also in the case of the mouse atrium, NIP-142, as well as tertiapin, a peptide inhibitor of the acetylcholine-activated potassium channel, prolonged the late repolarization phase (Figs. 2B, C). NIP-142 was shown to inhibit the acetylcholine-activated potassium channel current and prolong the action potential duration in guinea-pig atrial myocardium.[8] Thus, although further investigation is necessary for definitive conclusions, the most likely explanation for the effects of NIP-142 in mouse atria at present is that NIP-142 prolongs the atrial action potential duration through blockade of the transient outward current as well as the acetylcholine-activated potassium current, and produces prolongation of the effective refractory period.

Blockade of Kv1.5, Kv4.2 and Kv4.3 appears to be advantageous for the treatment of atrial fibrillation. It is well known that atrial arrhythmias are closely associated with pathological conditions including atrial dilatation.[16] Atrial

stretch exerts short-term and long-term effects on ion channel expression leading to shortening of the action potential duration and refractory period.[17] It was reported that 4-aminopyridine could counteract the shortening of action potential duration and effective refractory period induced by application of stretch to atrial myocytes.[18] Many studies support the hypothesis that in patients of atrial fibrillation, loss of atrial contractile function causing stasis of blood near the atrial wall is one of the important mechanisms of atrial thrombus formation.[19,20] Blockade of the transient outward current may be an effective strategy to inhibit atrial thrombus formation if it could increase atrial contractility. It was indeed reported that AVE0118, a blocker of the transient outward and ultrarapid delayed rectifier current, fully restored atrial contractility after cardioversion of atrial fibrillation in the goat without proarrhythmic effects on the ventricle.[21] In the present study, 1 mM 4-aminopyridine, which blocks the Kv1.5 channel current, and 10 mM 4-aminopyridine, which also blocks the Kv4.2 and Kv4.3 channel currents, gradually increased the atrial contractile force. Although details await further investigation, NIP-142, which prolonged action potential duration and increased atrial contractile force through inhibition of these currents, might also have these beneficial effects.

In conclusion, NIP-142 was shown to inhibit the Kv1.5, Kv4.2 and Kv4.3 channel current. This effect, and the blockade of acetylcholine-activated potassium current, may contribute to the prolongation of effective refractory period by NIP-142.

Acknowledgments This study was supported in part by the Science Research Promotion Fund from the Promotion and Mutual Aid Corporation for Private Schools of Japan (for YT and HT). This study was partly performed as a part of the project "Research on the molecular mechanisms of appearance of age-related diseases by failure of cell function control system, and their prevention and treatment" by the "Research Center for Aging and Age-Related Diseases" established in the Toho University Faculty of Pharmaceutical Sciences.

REFERENCES

1) Sugimoto T., Hayakawa K. and Kasanuki H., "Atrial Fibrillation, Flutter, and Tachycardia," ed. by Hayakawa K., Kasanuki H., Igaku-Shoin, Tokyo, 1999, pp. 14—18.
2) Aliot E., Denjoy I., *Am. J. Cardiol.*, 77, 66A—71A (1996).
3) Iwasaki H., Takahara A., Nakamura Y., Satoh Y., Nagai T., Shinkai N., Sugiyama A., *J. Pharmacol. Sci.*, **110**, 410—414 (2009).
4) Lenz T., Hilleman D., *Drugs Today* (Barc), **36**, 759—771 (2000).
5) Nagasawa H., Fujiki A., Fujikura N., Matsuda T., Yamashita T., Inoue H., *Circ. J.*, **66**, 185—191 (2002).
6) Matsuda T., Takeda K., Ito M., Yamagishi R., Tamura M., Nakamura H., Tsuruoka N., Saito T., Masumiya H., Suzuki T., Iida-Tanaka N., Itokawa M., Yamashita T., Tsuruzoe N., Tanaka H., Shigenobu K., *J. Pharmacol. Sci.*, **98**, 33—40 (2005).
7) Seki A., Hagiwara N., Kasanuki H., *J. Cardiovasc. Pharmacol.*, **39**, 29—38 (2002).
8) Matsuda T., Ito M., Ishimaru S., Tsuruoka N., Saito T., Iida-Tanaka N., Hashimoto N., Yamashita T., Tsuruzoe N., Tanaka H., Shigenobu K., *J. Pharmacol. Sci.*, **101**, 303—310 (2006).
9) Nishimaru K., Makuta R., Tanaka Y., Tanaka H., Shigenobu K., *Pharmacology*, **62**, 87—91 (2001).
10) Matsuda T., Masumiya H., Tanaka N., Yamashita T., Tsuruzoe N., Tanaka Y., Tanaka H., Shigenobu K., *Life Sci.*, **68**, 2017—2024 (2001).
11) Gaborit N., Bouter S.L., Szuts V., Varro A., Escande D., Nattel S., Demolombe S., *J. Physiol.*, **582**, 675—693 (2007).
12) Trépanier-Boulay V., Lupien M., St-Michel C., Fiset C., *Cardiovasc. Res.*, **64**, 84—93 (2004).
13) Wang Y., Xu H., Kumar R., Tipparaju S. M., Wagner M. B., Joyner R. W., *J. Mol. Cell. Cardiol.*, **35**, 1083—1092 (2003).
14) Oudit G. Y., Kassiri Z., Sah R., Ramirez R. J., Zobel C., Backx P. H., *J. Mol. Cell. Cardiol.*, **33**, 851—872 (2001).
15) Tanaka H., Namekata I., Nouchi H., Shigenobu K., Kawanishi T., Takahara A., *J. Pharmacol. Sci.*, **109**, 327—333 (2009).
16) Fukuda T., Yamashita T., Sagara K., Kato T., Sawada H., Aizawa T., *Circ. J.*, **71**, 308—312 (2007).
17) Kalifa J., Jalife J., Zaitsev A. V., Bagwe S., Warren M., Moreno J., Berenfeld O., Nattel S., *Circulation*, **108**, 668—671 (2003).
18) Qi J., Xiao J., Zhang Y., Li J., Liu Y., Li P., Liang L., Jiang B., Wen W., Zhao C., Liang D., Liu Y., Chen Y. H., *Exp. Biol. Med.*, **234**, 779—784 (2009).
19) Fatkin D., Kelly R. P., Feneley M. P., *J. Am. Coll. Cardiol.*, **23**, 961—969 (1994).
20) Mugge A., Kuhn H., Nikutta P., Grote J., Lopez J. A., Daniel W. G., *J. Am. Coll. Cardiol.*, **23**, 599—607 (1994).
21) deHaan S., Greiser M., Harks E., Blaauw Y., Hunnik A., Verheule S., Allessie M., Schotten U., *Circulation*, **114**, 1234—1242 (2006).

H_2 Receptor-Mediated Positive Inotropic Effect of Histamine in Neonatal Guinea-Pig Left Atria

Naoki AGATA,[a] Yoshimitsu KATO,[a] Iyuki NAMEKATA,[a] Akira TAKAHARA,[a] Hikaru TANAKA,*[,a] Daisuke CHINO,[b] Katsuo KOIKE,[c] and Yoshio TANAKA[c]

[a] *Department of Pharmacology, Faculty of Pharmaceutical Sciences, Toho University;* [c] *Department of Chemical Pharmacology, Faculty of Pharmaceutical Sciences, Toho University; Funabashi, Chiba 274–8510, Japan; and* [b] *Department of Pharmacology, School of Medicinal Pharmacy, Nihon Pharmaceutical University; Kitaadachi-gun, Saitama 362–0806, Japan.* Received August 20, 2010; accepted September 4, 2010; published online September 8, 2010

The receptor type mediating the positive inotropic effect of histamine was examined in left atria from neonatal guinea pigs. The positive inotropic effect of histamine, as well as its action potential prolonging effect, was antagonized by ranitidine, but not by chlorpheniramine or thiperamide. The positive inotropic effect was enhanced by isobutylmethylxantine. Receptor binding studies revealed the presence of both H_1 and H_2 receptor types. These results suggest that the positive inotropic effect of histamine in the neonatal guinea-pig atrium is mediated by H_2 receptors.

Key words histamine; inotropy; guinea-pig; left atrium; neonate

Histamine is present in high concentrations in the myocardium of most animal species including human, and its release and subsequent actions on the myocardium is considered to be of importance under certain pathological conditions such as arrhythmia and septic shock.[1—4] Histamine is known to produce increase in sinus rate and ventricular automaticity, a decrease in atrio-ventricular conduction velocity, and an increase in myocardial contractility through its direct action on cardiomyocytes. In some cases, histamine influences myocardial contractility through release of transmitters from autonomic nerve terminals.[5,6] The direct positive chronotropic and inotropic effects of histamine are principally mediated by activation of H_2 receptors and an increase in intracellular cAMP production, mechanisms analogous to that for β-adrenergic stimulation. However, there seems to be some variation in the type of receptors mediating the positive inotropic effect among animal species, region of the heart, as are often observed with other biologically active substances.[7,8] In case of the adult guinea-pig left atria, histamine shows a positive inotropic effect; this effect was shown to be mediated by H_1 receptors and to be accompanied by prolongation of the action potential.[9—12] The sensitivity to histamine of the left atria was reported to be low in the neonate and to be increased during postnatal development,[13] but whether there are any changes in the mechanisms involved has not yet been clarified. In the present study, we intended to clarify the receptor type involved in the positive inotropic effect of histamine on neonatal atria with contractile force experiments, action potential measurements, and receptor binding assay.

MATERIALS AND METHODS

Experiments with Isolated Guinea-Pig Atria All experiments were approved by the Ethics Committee of Toho University, and were performed in accordance with the "Guiding Principles for the Care and Use of Laboratory Animals" approved by the Japanese Pharmacological Society. The left atria were isolated from neonatal (0 to 1 d old) guinea pigs and measurement of the action potential with standard glass microelectrode techniques and measurement of contractile force were performed as described.[14,15] Briefly, the left atria were placed horizontally in 20 ml organ bath and driven at 1 Hz by field stimulation. Contractile force was measured with an isometric transducer (TB-611T, Nihon Kohden, Tokyo, Japan) connected to a minipolygraph (RM-6100, Nihon Kohden, Tokyo, Japan). Action potentials were recorded with glass microelectrodes connected to a microelectrode amplifier (MEZ-7101, Nihon Kohden, Tokyo, Japan), fed into an AD converter (Analog Pro, Canopus, Kobe, Japan) and digitally analyzed (Analy X, Sawada & Hirano, Tsukuba, Japan).

Preparation of Microsomal Fractions The atria removed from neonatal (0 to 1 d old) guinea-pigs were minced with scissors and homogenized with a Potter–Elveheim homogenizer in 20 volume of 0.25 M sucrose containing 10 mM tris(hydroxymethyl)aminomethane–HCl (Tris–HCl; pH 7.4 at 4 °C). The homogenate was centrifuged at 2500 ***g*** for 10 min and the supernatant was again centrifuged at 15000 ***g*** for 20 min. Centrifugation of this supernatant at 100000 ***g*** for 60 min resulted in a pellet that was suspended in 10 mM Tris–HCl at a concentration of 0.5 to 0.8 mg protein/ml and was used as the microsomal fraction.

Receptor Binding Assay The microsomal fraction was incubated with various concentrations of [^{3}H]mepyramine or [^{3}H]tiotidine in a total volume of 150 μl of incubation buffer (50 mM Tris–HCl, pH 7.4 at 37 °C) for 60 min. The incubation mixture was filtered with Whatman GF/C glass-fiber filters. After the passage, the filters were dried and the radioactivity was measured in a toluene-based scintillator with a liquid scintillation spectrometer (LSC-900, Aloka, Tokyo, Japan). Non-specific binding was determined as radioactivity bound to the microsomal fraction that was not displaced by non-radioactive ligands (30 μM mepyramine or 10 μM cimetidine). Specific binding was obtained as the difference between total binding and non-specific binding. The maximum binding capacity (B_{max}) and the equilibrium dissociation constant (K_d) were calculated from Scatchard analysis of the saturation data.

Drug and Chemicals The drugs used were histamine di-

* To whom correspondence should be addressed. e-mail: htanaka@phar.toho-u.ac.jp

hydrochloride (Wako, Osaka, Japan), chlorpheniramine maleate (Wako, Osaka, Japan), ranitidine hydrochloride (Sigma-Aldrich, St. Louis, MO, U.S.A.), cimetidine (Sigma-Aldrich, St. Louis, MO, U.S.A.), thioperamide maleate (Sigma-Aldrich, St. Louis, MO, U.S.A.), 3-isobutyl-1-methylxanthine (IBMX; Sigma-Aldrich, St. Louis, MO, U.S.A.), ^{3}H-mepyramine (PerkinElmer, Waltham, MA, U.S.A.), and ^{3}H-tiotidine (PerkinElmer, Waltham, MA, U.S.A.). All other chemicals were commercial products of the highest available grade of quality.

Statistical Analysis All experimental data are expressed as mean±standard errors of the mean (S.E.M.). The statistical significance of differences between means was evaluated by the Dunnett's test for multiple comparisons. A value of $p<0.05$ was considered statistically significant.

RESULTS

In isolated neonatal guinea-pig left atria, histamine produced a concentration-dependent positive inotropic effect (Fig. 1A); the pD_2 value was 5.29±0.12 and the contractile force was increased to 253±19.1% of the initial value by 10 μM histamine ($n=5$). The H_2 receptor antagonist ranitidine produced a rightward shift of the concentration–response relationship of histamine. The pD_2 value in the presence of 10 μM ranitidine was 3.81±0.19 ($n=5$) and the calculated pA_2 value was 6.46. In contrast, neither the H_1 antagonist chlorpheniramine nor the H_3 receptor antagonist thioperamide affected the concentration–response relationship; pD_2 values in the presence of 0.3 μM chlorpheniramine and 1 μM thiperamide were 5.04±0.05 and 5.36±0.12, respectively. The phosphodiesterase inhibitor isobutylmethylxantine (IBMX) enhanced the inotropic response to histamine (Fig. 1B).

Histamine prolonged the action potential duration (Fig. 2Aa). The action potential duration at 90% repolarization (APD_{90}) in the absence and presence of 3 μM histamine was 81.6±3.7 ms and 101.0±3.3 ms, respectively ($n=5$). This prolongation of APD_{90} by histamine was abolished by 10 μM ranitidine, but not by 0.3 μM chlorpheniramine or 1 μM thiperamide (Fig. 2B).

Receptor binding assay with microsomal preparations from neonatal atria revealed the presence of binding sites for both the H_1 antagonist mepyramine and the H_2 receptor antagonist tiotidine. The maximum binding capacity (B_{max}) and dissociation constant (K_d) for mepyramine were 177.2±6.2 fmol/mg protein and 0.49±0.06, respectively ($n=4$), and those for tiotidine were 93.1±11.3 fmol/mg protein and 14.8±6.8, respectively ($n=4$).

DISCUSSION

The positive inotropic effect of histamine in neonatal guinea-pig left atria was antagonized by ranitidine (Fig. 1A). The observed pA_2 value of 6.46 was close to the reported pA_2 value of ranitidine against H_2 receptors in human atria.[16] In contrast, neither the H_1 antagonist chlorpheniramine nor the H_3 receptor antagonist thioperamide affected the positive inotropic effect. These results indicate that the positive inotropic effect of histamine on neonatal left atria is mediated by H_2 receptors. It is generally known that stimulation of H_2 receptors induces physiological responses through increase in cAMP concentration. The present result that the histamine-induced positive inotropy was enhanced by IBMX (Fig. 1B) suggests that this is the case with neonatal guinea-pig left atria.

Histamine prolonged the action potential duration in neonatal left atria through stimulation of H_2 receptors (Fig.

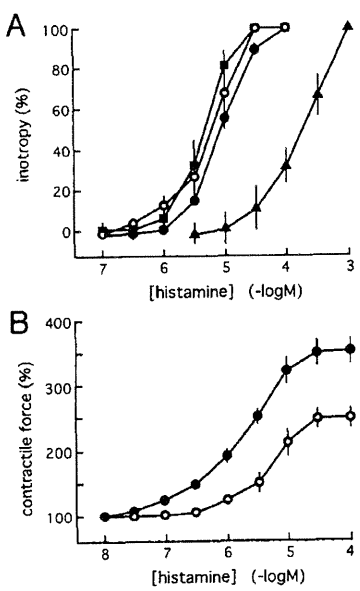

Fig. 1. Effects of Pharmacological Agents on the Histamine-Induced Positive Inotropy in Neonatal Guinea-Pig Left Atria

(A) Concentration–response relationship of histamine in the absence (open circles) and presence of receptor antagonists chlorpheniramine (0.3 μM; closed circles), ranitidine (10 μM; closed triangles) and thioperamide (1 μM, closed squares). Increase in contractile force after addition of each concentration was expressed as a percentage of the maximum increase. (B) Effect of isobutylmethylxantine (1 μM). Increase in contractile force after addition of each concentration was expressed as a percentage of the basal contractile force. Data points and vertical bars in A and B represent the mean±S.E.M. from 5 experiments

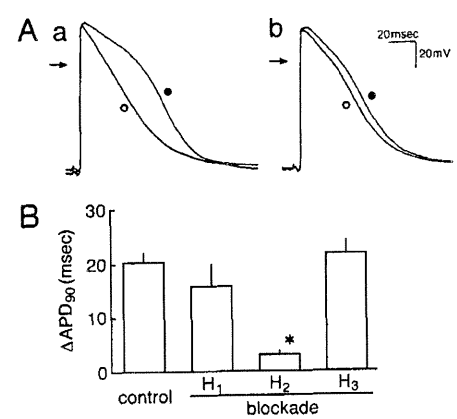

Fig. 2. Effect of Histamine on the Action Potential of Neonatal Guinea-Pig Left Atria

(A) Typical action potential records obtained before (open circles) and after (closed circles) the addition of histamine (10 μM) in the absence (a) and presence (b) of ranitidine (10 μM). Arrows indicate zero mV level. (B) Summarized results of the prolongation of action potential duration at 90% repolarization (APD_{90}). Columns and vertical bars represent the mean±S.E.M. from 5 experiments. The asterisks indicate statistical significance against the control value.

2). Such prolongation was also observed in adult left atria. The prolongation was mediated through H_1 receptors and inhibition of outward currents.[11,12] As the action potential properties of the guinea pig myocardium changes during postnatal development,[14,17] the ionic mechanisms, as well as the receptor type, for prolongation of the action potential by histamine may be different between the adult and neonatal left atria.

Receptor binding assay revealed the presence of both H_1 and H_2 receptors in the neonatal left atria. This means that, although two types of receptors are present, only the H_2 receptor is coupled to mechanisms leading to positive inotropy. In the adult left atria, both H_1 and H_2 receptors are present but only the H_1 receptor is coupled to positive inotropy. Thus, the receptors responsible for the histamine-induced inotropy change from H_2 to H_1 during postnatal development. Various properties in the excitation and contraction, as well as in the signal transduction mechanisms occur during myocardial development.[8] The intracellular mechanisms underlying the developmental shift from H_2 receptor-mediated to H_1 receptor-mediated inotropy in the guinea-pig left atria await further investigation. While it is established that H_2 receptor stimulation results in increased cAMP production, evidence both for[18] and against[19] the role of phosphoinositide hydrolysis in response to H_1 receptor stimulation has been reported. Clarification of the precise mechanisms for the H_1 receptor-mediated inotropy, as well as the developmental shift from H_2 to H_1, would contribute to the understanding of signal transduction mechanisms. Diminution of H_2 receptor-mediated inotropy was also reported in the developing chick ventricular myocardium.[20]

In conclusion, the present study revealed that the receptor type mediating the positive inotropy in the guinea-pig left atrial myocardium is converted from H_2 to H_1 during postnatal development. The present findings imply that the histamine-mediated mechanisms in the myocardium may change during postnatal development.

Acknowledgments This study was supported in part by the Science Research Promotion Fund from the Promotion and Mutual Aid Corporation for Private Schools of Japan (for YT and HT). This study was partly performed as a part of the project "Research on the molecular mechanisms of appearance of age-related diseases by failure of cell function control system, and their prevention and treatment" by the "Research Center for Aging and Age-Related Diseases" established in the Toho University Faculty of Pharmaceutical Sciences.

REFERENCES

1) McNeill J. H., *Can. J. Physiol. Pharmacol.*, **62**, 720—726 (1984).
2) Wolff A. A., Levi R., *Circ. Res.*, **58**, 1—16 (1986).
3) Hattori Y., *Methods Find. Exp. Clin. Pharmacol.*, **21**, 123—131 (1999).
4) Matsuda N., Hattori Y., Sakuraya F., Kobayashi M., Zhang X.-H., Kemmotsu O., Gando S., *Naunyn-Schmied. Arch. Pharmacol.*, **366**, 513—521 (2002).
5) Laher I. E., McNeill J. H., *Can. J. Physiol. Pharmacol.*, **58**, 1256—1261 (1980).
6) Tanaka H., Uesato N., Shigenobu K., *Naunyn-Schmied. Arch. Pharmacol.*, **352**, 626—630 (1995).
7) Endoh M., *J. Pharmacol. Sci.*, **100**, 525—537 (2006).
8) Tanaka H., Namekata I., Nouchi H., Shigenobu K., Kawanishi T., Takahara A., *J. Pharmacol. Sci.*, **109**, 327—333 (2009).
9) Levi R., Allan G., Zavecz J. H., *Fed. Proc. Fed. Am. Soc. Exp. Biol.*, **35**, 1942—1947 (1976).
10) Verma S. C., McNeill J. H., *J. Pharmacol. Exp. Ther.*, **200**, 352—362 (1977).
11) Hattori Y., Endou M., Gando S., Kanno M., *Br. J. Pharmacol.*, **103**, 1573—1579 (1991).
12) Yoshimoto K., Hattori Y., Houzen H., Kanno M., Yasuda K., *Br. J. Pharmacol.*, **124**, 1774—1750 (1998).
13) Shigenobu K., Sawada K., Kasuya Y., *Can. J. Physiol. Pharmacol.*, **58**, 1300—1306 (1980).
14) Agata N., Tanaka H., Shigenobu K., *Acta Physiol. Scand.*, **149**, 331—337 (1993).
15) Agata N., Tanaka H., Shigenobu K., *Eur. J. Pharmacol.*, **260**, 47—55 (1994).
16) Poli E., Medici D., Contini G. A., Bertaccini G., *Arch. Int. Pharmacodyn. Ther.*, **273**, 221—225 (1985).
17) Kato Y., Tanaka H., Shigenobu K., *J. Mol. Cell. Cardiol.*, **28**, 1515—1522 (1996).
18) Sakuma I., Gross S. S., Levi R., *J. Pharmacol. Exp. Ther.*, **247**, 466—472 (1988).
19) Hattori Y., Endou M., Shirota M., Kanno M., *Naunyn-Schmied. Arch. Pharmacol.*, **340**, 196—203 (1989).
20) Tanaka H., Uesato N., Shigenobu K., *Naunyn-Schmied. Arch. Pharmacol.*, **351**, 391—357 (1995).

Biochemical and Biophysical Research Communications 398 (2010) 284–289

Contents lists available at ScienceDirect

Biochemical and Biophysical Research Communications

journal homepage: www.elsevier.com/locate/ybbrc

Role of transient receptor potential vanilloid 2 in LPS-induced cytokine production in macrophages

Kenji Yamashiro [a,b,c], Tetsuo Sasano [d], Katsuyoshi Tojo [a], Iyuki Namekata [f], Junko Kurokawa [b], Naoki Sawada [c,d], Takayoshi Suganami [c], Yasutomi Kamei [c], Hikaru Tanaka [f], Naoko Tajima [a], Kazunori Utsunomiya [a], Yoshihiro Ogawa [c,e,*], Tetsushi Furukawa [b,**]

[a] Division of Diabetes and Endocrinology, Department of Internal Medicine, Jikei University School of Medicine, 1-5-45 Yushima, Bunkyo-ku, Tokyo 113-8510, Japan
[b] Department of Bio-informational Pharmacology, 1-5-45 Yushima, Bunkyo-ku, Tokyo 113-8510, Japan
[c] Department of Molecular Medicine and Metabolism, 1-5-45 Yushima, Bunkyo-ku, Tokyo 113-8510, Japan
[d] Medical Top Track Program, 1-5-45 Yushima, Bunkyo-ku, Tokyo 113-8510, Japan
[e] Global Center of Excellence Program, International Research Center for Molecular Science in Tooth and Bone Diseases, Medical Research Institute, Tokyo Medical and Dental University, 1-5-45 Yushima, Bunkyo-ku, Tokyo 113-8510, Japan
[f] Department of Pharmacology, Toho University Faculty of Pharmaceutical Sciences, 1-5-45 Yushima, Bunkyo-ku, Tokyo 113-8510, Japan

ARTICLE INFO

Article history:
Received 2 June 2010
Available online 23 June 2010

Keywords:
Transient receptor potential vanilloid 2
Macrophage
LPS
Cytokine
Calcium

ABSTRACT

There is considerable evidence indicating that intracellular Ca^{2+} participates as a second messenger in TLR4-dependent signaling. However, how intracellular free Ca^{2+} concentrations ($[Ca^{2+}]_i$) is increased in response to LPS and how they affect cytokine production are poorly understood. Here we examined the role of transient receptor potential (TRP), a major Ca^{2+} permeation pathway in non-excitable cells, in the LPS-induced cytokine production in macrophages. Pharmacologic experiments suggested that TRPV family members, but neither TRPC nor TRPM family members, are involved in the LPS-induced TNFα and IL-6 production in RAW264 macrophages. RT-PCR and immunoblot analyses showed that TRPV2 is the sole member of TRPV family expressed in macrophages. ShRNA against TRPV2 inhibited the LPS-induced TNFα and IL-6 production as well as IκBα degradation. Experiments using BAPTA/AM and EGTA, and Ca^{2+} imaging suggested that the LPS-induced increase in $[Ca^{2+}]_i$ involves both the TRPV2-mediated intracellular and extracellular Ca^{2+} mobilizations. BAPTA/AM abolished LPS-induced TNFα and IL-6 production, while EGTA only partially suppressed LPS-induced IL-6 production, but not TNFα production. These data indicate that TRPV2 is involved in the LPS-induced Ca^{2+} mobilization from intracellular Ca^{2+} store and extracellular Ca^{2+}. In addition to Ca^{2+} mobilization through the IP_3-receptor, TRPV2-mediated intracellular Ca^{2+} mobilization is involved in NFκB-dependent TNFα and IL-6 expression, while extracellular Ca^{2+} entry is involved in NFκB-independent IL-6 production.

1. Introduction

Macrophages are a central player of innate immunity and inflammation. They are capable of producing a variety of proinflammatory cytokines such as TNFα and IL-6 following Lps stimulation [1,2]. Intracellular signaling pathways downstream of TLR4 stimulation by LPS have been extensively studied [1,2]. Upon LPS stimulation, TLR4 initiates a series of NFκB- and MAPK-associated intracellular signaling events, thereby inducing the expression of an array of proinflammatory cytokine genes.

Intracellular free Ca^{2+} concentrations ($[Ca^{2+}]_i$) or Ca^{2+} fluxes are important for cellular responses to extracellular stimuli [3,4]. There is considerable evidence that intracellular Ca^{2+} participates as a second messenger in TLR4-dependent signaling [5]. Indeed, treatment with LPS causes a transient increase in $[Ca^{2+}]_i$, which is required for increased TNFα production in macrophages [6]. However, the molecular mechanisms by which LPS increases $[Ca^{2+}]_i$ and how the LPS-induced Ca^{2+} fluxes modulates proinflammatory cytokine production are still poorly understood.

Transient receptor potential (TRP) channels are a group of Ca^{2+}-permeable channels with diverse activation properties including temperature, pH changes, ADP-ribose, and diacylglycerol [7]. TRP channels are suggested to be an important Ca^{2+} entry pathway in non-excitable cells [7]. For instance, TRP vanilloid 4 (TRPV4)- and TRPV5-mediated Ca^{2+} influx is essential for terminal differentiation of osteoclasts and osteoclastic bone resorption [8,9]. Activation of the TRP melastatin 8 (TRPM8) variant in human lung epithelial cells also leads to increased expression of several cytokine and chemokine genes [10]. TRPV1 is expressed primarily in sensory nerves

* Corresponding author. Fax: +81 3 5803 4931.
** Corresponding author. Fax: +81 3 5803 4950.
E-mail addresses: ogawa.mmm@mri.tmd.ac.jp (Y. Ogawa), t_furukawa.bip@mri.tmd.ac.jp (T. Furukawa).

0006-291X/$ - see front matter © 2010 Elsevier Inc. All rights reserved.
doi:10.1016/j.bbrc.2010.06.082

and protects against the onset of LPS-induced sepsis [11]. Reactive oxygen species-induced chemokine production has been shown to be mediated through TRPM2-mediated Ca^{2+} influx in monocytes/macrophages [12]. However, whether TRP channels are involved in the LPS-induced Ca^{2+} mobilization in macrophages has not been addressed.

TRPV2 is a Ca^{2+} permeable channel originally identified in rat brain and human myeloid cell line, CCRF-CEM [13]. Here we provide *in vitro* evidence that TRPV2 is involved in LPS-induced Ca^{2+} mobilization and induction of cytokines in RAW macrophages. Our data will also help elucidate the molecular mechanisms underlying the LPS-induced cytokine production in macrophages and thus identify the therapeutic targets that may prevent or treat a variety of acute and chronic inflammatory diseases.

2. Materials and methods

2.1. Reagents

All reagents were purchased from Sigma–Aldrich (St. Louis, MO) or Nacalai Tesque (Kyoto, Japan). Rabbit mAbs against IκBα, and phospho-IκBα (Ser32) (p-IκBα) were purchased from Cell Signaling (Beverly, MA), and a rabbit polyclonal Ab against mouse TRPV2 (mTRPV2) from Abcam Inc. (Cambridge, MA).

2.2. Cell culture and transfection

A macrophages cell line RAW264 (RIKEN BioResource Center, Tsukuba, Japan), and HEK293T were maintained in DMEM (Nacalai Tesque, Kyoto, Japan) containing 10% FBS (BioWest, Miami, FL). To produce HEK293T cells expressing TRPV2, pcMV6-Kan/Neo-mTRPV2 (OriGene Technologies, RockVille, MD) was transfected by Lipofectamine™2000 (Invitrogen Life Technologies, CA). Murine bone marrow-derived macrophages were prepared as described [14].

2.3. Lentivirus short hairpin RNA (shRNA) vector construction and gene transduction

The construction of the shRNA for TRPV2 (NM_011706), and gene transduction were carried out as previously reported [15]. The sense and antisense oligonucleotides used are shown in Supplementary Table 1. Lentivirus-infected cells were detected as GFP-positive. After 4 weeks of selection, over 90% of cells were GFP-positive and used for further analysis.

2.4. Quantitative real-time RT-PCR analysis

Quantitative real-time RT-PCR was performed with SYBR Green PCR Master MixReagent Kit (Applied Biosystems, Foster City, CA) [16]. The primer sets used to detect each of TRPV members are shown in Supplementary Table 2.

2.5. Measurement of TNFα and IL-6 protein levels in culture media

The TNFα and IL-6 protein levels were determined by the commercially available enzyme-linked immunosorbent assay (ELISA) kits (R&D systems, Minneapolis, MN).

2.6. Immunoblot analysis

Immunoblot analysis was performed as described [16]. Membranes were immunoblotted with one of following primary Abs; p-IκBα (1:1000), IκBα (1:2000), α-tubulin (1:16,000), or mTRPV2 (1:500).

2.7. Measurement of $[Ca^{2+}]_i$ concentration

Measurement of $[Ca^{2+}]_i$ was performed with epifluorescent microscopy (Hamamatsu Photonics, Hamamatsu, Japan) as previously described [17]. Calibration between fluorescence ratio and Ca^{2+} concentration was performed *in situ* as described [18].

2.8. Statistical analysis

Data are expressed as the mean ± SEM. Statistical analysis was performed using Student's *t*-test. $P < 0.05$ was considered to be statistically significant.

3. Results

3.1. Effect of TRP channel blockers on the LPS-induced cytokine production in RAW264 and murine macrophages

Macrophages express several TRP channels including TRPC, TRPM, and TRPV family members [12,19]. To explore if TRP family members play a role in the LPS-induced inflammatory response, and if so, which TRP channel(s) are involved, we first used ruthenium red (RR), a non-selective TRP channel blocker [20], Gadolinium (Gd), a TRPC channel blocker at a low concentration (30 μM) and a TRPC and a TRPV channel blocker at a high concentration (1 mM) [20,21], and flufenamic acid (FFA), a TRPC and TRPM channel blocker [21,22]. Treatment with LPS at a dose of 5 ng/ml significantly increased TNFα and IL-6 mRNA expression ($P < 0.01$), which was markedly inhibited by RR (10 μM) (Fig. 1A). Treatment with Gd at a dose of 30 μM did not affect the LPS-induced TNFα and IL-6 mRNA expression (Fig. 1B), but, at a dose of 1 mM, it significantly inhibited the LPS-induced IL-6 mRNA expression ($P < 0.01$), but not TNFα mRNA expression (Fig. 1C). FFA (100 μM) did not affect the LPS-induced TNFα and IL-6 mRNA expression (Fig. 1D). Similarly, treatment with RR (10 μM) significantly suppressed the LPS-induced TNFα and IL-6 secretion ($P < 0.01$), while treatment with Gd at 1 mM inhibited the LPS-induced IL-6 secretion ($P < 0.01$), but not TNFα secretion (Supplementary Fig. 1).

We also examined effects of RR and Gd on the LPS-induced cytokine secretion from murine bone marrow-derived macrophages. RR (10 μM) significantly suppressed the TNFα and IL-6 secretion stimulated by LPS (10 ng/ml) for 6 h and 24 h ($P < 0.01$) (Fig. 1E). Gd (1 mM) suppressed IL-6 ($P < 0.05$), but not TNFα, secretion stimulated by LPS for 24 h (Fig. 1F).

These observations suggest that TRPV family members, but neither TRPC nor TRPM, are involved in the LPS-induced TNFα and IL-6 production in macrophages. Since the effects of RR and Gd are more prominent in RAW264, we used RAW264 in the following experiments.

3.2. Expression of TRPV2 in RAW264 macrophages

We examined expression of mRNAs for TRPV family members (TRPV1~6) in RAW264 macrophages. RT-PCR analysis revealed that TRPV2 mRNA is expressed in RAW264 macrophages (Fig. 2A). There were no appreciable amounts of mRNAs for TRPV1, 3, 4, 5, and 6. We examined TRPV2 protein expression in RAW264 macrophages. Immunoblot analysis identified two immunoreactive bands at ~110 and at ~85 kD (Fig. 2B), which may be the products of post-translational modification such as glycosylation and phosphorylation [23]. Expression of TRPV2 protein in RAW264 macrophages was further confirmed by the positive immune-staining with an anti-TRPV2 antibody in immune-cytochemical studies (Supplementary Fig. 2).